

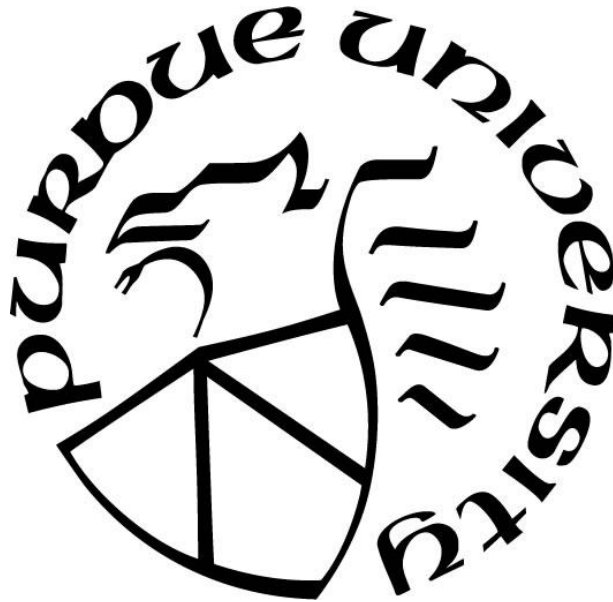
**MODELING AND SIMULATION OF CONVECTIVE HEAT TRANSFER  
CAUSED BY A ROTATING DISK**

by  
**David Ruiz**

**A Thesis**

*Submitted to the Faculty of Purdue University  
In Partial Fulfillment of the Requirements for the degree of*

**Master of Science in Engineering**



Department of Civil and Mechanical Engineering

Fort Wayne, Indiana

May 2020

**THE PURDUE UNIVERSITY GRADUATE SCHOOL**  
**STATEMENT OF COMMITTEE APPROVAL**

**Dr. Hosni Abu-Mulaweh, Co-Chair**

Department of Civil and Mechanical Engineering

**Dr. Donald Mueller, Co-Chair**

Department of Civil and Mechanical Engineering

**Dr. Safwan Akkari**

Department of Mathematics

**Approved by:**

Dr. Hosni Abu-Mulaweh

*For my parents who have always supported and guided me through life.  
For the friends I call my brothers and sisters who always pushed me to be the best I can be.*

## **ACKNOWLEDGMENTS**

Thanks, is extended to the advisors, Dr. Hosni Abu-Mulaweh and Dr. Donald Mueller, for their guidance throughout the last year. This included questions and comments to aid in conducting the study.

Thanks, is also extended to Dr. Safwan Akkari, for showing interest in the study and being a part of the committee.

# TABLE OF CONTENTS

LIST OF TABLES .....	7
LIST OF FIGURES .....	8
NOMENCLATURE .....	10
ABSTRACT.....	11
1. INTRODUCTION .....	12
1.1 Temperature and Velocity Profiles Due to Rotation for Verification of Model.....	12
1.2 Validation of the Simulation by Comparing to Analytical Solutions.....	14
1.3 Thesis Objectives .....	14
1.4 Thesis Organization .....	16
2. LITERATURE REVIEW .....	18
3. PROBLEM STATEMENT AND VERIFICATION OF MODEL.....	22
3.1 Problem Statement .....	22
3.1.1 Mathematical Modeling.....	23
3.1.2 Detailed Procedure to Create a Disk in SolidWorks .....	24
3.2 Verification of the Model.....	26
3.2.1 Velocity and Temperature Profiles.....	27
4. DESCRIPTIONS AND PROCEDURES FOR GLOBAL ROTATION METHOD AND LOCAL ROTATION (SLIDING) METHOD .....	34
4.1 Global Rotation Method: Description.....	34
4.1.1 Detailed Procedure for Global Rotation Method.....	34
4.2 Local Rotation (Sliding) Method: Description .....	40
4.2.1 Detailed Procedure for Local Rotation (Sliding) Method .....	40
5. COMPARISON BETWEEN THE GLOBAL ROTATION AND LOCAL ROTATION (SLIDING) METHODS.....	44
6. TESTING FOR FULL RANGE OF ROTATIONAL SPEEDS .....	55
6.1 Description of Rotational Regimes for Different Reynolds Number .....	55
6.1.1 Detailed Procedure for Various Rotational Speeds .....	57
6.2 Validation of Various Rotational Rates .....	58

7. IMPACT OF TOTAL AMOUNT OF CELLS ON SIMULATION TIME AND EXPECTED PERCENT DIFFERENCE .....	68
8. CONCLUSION.....	72
REFERENCES .....	75

## LIST OF TABLES

Table 3.1: Summary of the locations used to verify the CFD simulation.....	28
Table 5.1: Parametric study input variables for both methods .....	45
Table 5.2: Summary of the results for both methods when the initial mesh level is set at 1.....	46
Table 5.3: Summary of the results for both methods when the initial mesh level is set at 2.....	47
Table 5.4: Summary of the results for both methods when the initial mesh level is set at 3.....	49
Table 5.5: Summary of the results for both methods when the initial mesh level is set at 4.....	50
Table 5.6: Parametric study input variables.....	52
Table 5.7: Flow regime boundaries .....	52
Table 5.8: Global rotation results at higher angular velocities and level of initial mesh of 5 .....	53
Table 5.9: Summary of global rotation method results near the beginning of the laminar regime .....	54
Table 5.10: Summary of global rotation method results near the end of the laminar regime .....	54
Table 6.1: Rotational Reynolds number for each flow regime for a rotating disk in still air .....	55
Table 6.2: Parametric study input variables for turbulent simulations .....	59
Table 6.3: Summary of global rotation method results at low, turbulent Reynolds number .....	60
Table 6.4: Summary of global rotation method results at higher, turbulent Reynolds number....	61
Table 7.1: Expected times and percent differences for the meshes tested in the laminar regime	69
Table 7.2: Expected times and percent differences for the meshes tested in the turbulent regime .....	70

## LIST OF FIGURES

Figure 1.1: Velocity and temperature profiles over a rotating disk in still air.....	13
Figure 1.2: Geometry for a rotating disk created in SolidWorks.....	15
Figure 3.1: Dimensions of the disk created in SolidWorks .....	22
Figure 3.2: How to quickly change the document units once SolidWorks is opened .....	24
Figure 3.3: Begin the sketch on the top plane to create the disk geometry within SolidWorks ...	25
Figure 3.4: Basic geometry of the disk with the center at the origin and diameter of 1 m.....	25
Figure 3.5: Final geometry of the disk including the dimensions all in meters.....	26
Figure 3.6: Plot showing the full range for a temperature profile .....	28
Figure 3.7: Dimensionless velocity profile at various locations along the surface of the disk.....	29
Figure 3.8: Dimensionless temperature profile plot for various rotational rates .....	30
Figure 3.9: Dimensionless temperature profile plot to show the effects as radial position changes .....	30
Figure 3.10: Dimensionless velocity profile plot for various rotational rates .....	32
Figure 3.11: Dimensionless velocity profile plot to show the effects as radial position changes	32
Figure 4.1: Project wizard first pop-up screen used to name the CFD simulation file.....	35
Figure 4.2: Units selected for the CFD simulation .....	35
Figure 4.3: Settings for the CFD simulation.....	36
Figure 4.4: Fluid selected for the initial CFD simulation .....	36
Figure 4.5: Temperature of the disk within the CFD simulation.....	37
Figure 4.6: Initial and ambient conditions used during the global rotation method.....	37
Figure 4.7: The computational size and conditions used within the CFD analysis and simulation .....	38
Figure 4.8: Selected surfaces of the disk which have the local mesh generated .....	38
Figure 4.9: Setting of the local mesh .....	39
Figure 4.10: Adiabatic boundary conditions for the bottom and side of the disk.....	39
Figure 4.11: Secondary body generated to create the local rotating domain.....	41
Figure 4.12: Settings for global rotation method and the local rotation (sliding) method.....	42
Figure 4.13: Angular velocity assigned to the secondary body generated .....	42

Figure 5.1: Global mesh settings used during each set of simulations .....	44
Figure 5.2: Local mesh settings used during each set of simulations .....	44
Figure 5.3: Results obtained for the both methods using a level of the initial mesh size of 1 .....	45
Figure 5.4: Results obtained for the both methods using a level of the initial mesh size of 2 .....	47
Figure 5.5: Results obtained for the both methods using a level of the initial mesh size of 3 .....	48
Figure 5.6: Results obtained for the both methods using a level of the initial mesh size of 4 .....	50
Figure 5.7: Higher angular velocities tested with a level of the initial mesh size of 5 .....	52
Figure 6.1: Available options for the flow type when initializing the CFD simulation .....	55
Figure 6.2: Default settings for the two definitions of the turbulence parameters .....	56
Figure 6.3: Turbulence parameters used for the turbulent simulation .....	57
Figure 6.4: Setting used to change the mesh size for each simulation conducted .....	58
Figure 6.5: Turbulent results obtained for initial mesh level of 1 and 2 .....	60
Figure 6.6: Summary of results for both laminar and turbulent regime .....	63
Figure 6.7: Flow type settings for the transition zone simulations .....	64
Figure 6.8: Turbulent parameters settings when simulating the transition zone .....	64
Figure 6.9: The dependency types available in SolidWorks CFD .....	65
Figure 6.10: Simulation showing convergence in transition zone .....	65
Figure 6.11: Results for all regimes .....	66
Figure 7.1: Laminar relation of the total number of cells and the simulation time .....	68
Figure 7.2: Laminar relation of the total number of cells and the expected percent difference ...	69
Figure 7.3: Turbulent relation of the total number of cells and the simulation time .....	71
Figure 7.4: Turbulent relation of the total number of cells and the expected percent difference .	71

## NOMENCLATURE

$C$	General Nusselt number correlation constant
$C_m$	Average Nusselt number correlation constant for rotation
$e_{ijk}$	Levy-Crivita function
$\bar{h}$	Average heat transfer coefficient (W/ (m <sup>2</sup> .K))
$k$	Thermal conductivity (W/ (m.K))
$n$	Nusselt number correlation exponent value
$Nu$	General average Nusselt number
$Nu_R$	Average Nusselt number based on the radius for rotation
$R$	Radius of the disk (m)
$r$	Radial position (m)
$r_i$	Radial distance for $i = 1, 2, 3$ (m)
$Re$	General Reynolds number
$Re_\omega$	Reynolds number based on the angular velocity and radius
$S_i^{rotation}$	Force due to rotation for $i = 1, 2, 3$ (N)
$T$	Temperature at any location (K)
$T_\infty$	Ambient temperature of the fluid (K)
$T_w$	Wall temperature of the surface of the disk (K)
$u_k$	Velocity component in the k direction (m/s)
$V$	Tangential velocity (m/s)
$ V $	In-plane velocity of the fluid (m/s)
$V^*$	Dimensionless in-plane velocity
$V_x$	X-component of the fluid's velocity (m/s)
$V_z$	Z-component of the fluid's velocity (m/s)
$x$	x-axis
$y$	y-axis
$z$	z-axis
$\theta^*$	Dimensionless temperature
$\nu$	Kinematic viscosity (m <sup>2</sup> /s)
$\rho$	Density (kg/m <sup>3</sup> )
$\omega$	Angular velocity (rad/s)

## ABSTRACT

Convective heat transfer due to the rotation of a submerged disk has applications ranging from the design of disk brakes, turbomachinery, and the wheels of a train. Within this study, computational fluid dynamics (CFD) software is utilized to analyze a smooth disk rotating in still fluid. To ensure the physical properties of the situation are captured, the temperature and velocity profiles of the fluid are verified to match the results reported in the literature. For a rotating disk, both temperature and velocity profiles must approach a minimum value of zero at heights far from the surface of the disk and a maximum value near the surface of the disk. By studying the velocity and temperature profiles, an estimate for the proper size of the computational domain within the CFD software is obtained. The size of the computational domain, when too small, can impact the results of the convective heat transfer coefficient due to the boundary disrupting the fluid. Within the CFD software, two methods can be utilized to obtain results for the convective heat transfer coefficient. The methods being, the global rotation method, and the local rotation (sliding) method. A comparison between the two methods and the expected heat transfer coefficient values predicted by correlations found in previous works of literature allows for the validation of the CFD software. Both methods agree with the expected heat transfer coefficient value and show agreement by maintaining a percent difference below three percent for low angular velocities. The global rotation method is best suited for a singular disk rotating in still air. When testing for faster angular speeds, the global rotation method was utilized and maintained low percent differences, below three percent, once an appropriate mesh was established and the turbulent parameters were set correctly. By having results that agree with correlations from previous literature, CFD software, once verified and validated, is a viable option when designing disk brakes, turbomachinery, and the wheels of a train.

# 1. INTRODUCTION

Convective heat transfer classifications include forced, natural, and mixed convection. In all three types of convective heat transfer, the main goal is to determine the convective heat transfer coefficient of the fluid. An external source causes the fluid's motion in forced convection. Natural convection, in contrast, does not have an external source causing the fluid's motion. During natural convection, the source of the fluid's motion is the density differences present due to temperature gradients in the fluid. Mixed convection is a combination of both natural and forced convection. Indicating that both the velocity of the fluid and the density of the fluid must be considered, and neither can be neglected.

When first studying forced convection, many of the examples shown are fluids moving across a plate or a stationary object, and the goal of the example is to determine the heat transfer coefficient of the fluid. However, the fluid's motion in forced convection does not necessarily need to be caused by an entirely external source. Instead, the fluid's motion can be caused by an object submerged in the fluid, such as a rotating disk. Heat transfer caused by a rotating body can be understood by utilizing computers, especially computational fluid dynamics (CFD) software.

## 1.1 Temperature and Velocity Profiles Due to Rotation for Verification of Model

The utilization of CFD software to determine the forced convective heat transfer coefficient over a rotating flat disk is the focus of this study. However, when creating a CFD model and simulation, there must be a process to verify the model generated in the CFD software and a process to validate the results obtained from the CFD simulation. Before creating a CFD model, one must understand the general behavior of the disk and the fluid surrounding the disk, as this can be used to verify the model is appropriately representing the problem. A possible item to analyze for verification is the fluid velocity on the surface of the disk. At the surface of the disk, the fluid's velocity is the same as the tangential velocity. The relation between the tangential velocity and the angular velocity can be shown as

$$V = \omega r. \tag{1.1}$$

Additionally, when placing the rotating disk within a still fluid, the velocity of the fluid must be maximum at the surface of the disk and minimum at locations far from the disk. If the temperature of the disk is higher than the temperature of the surrounding fluid, then the fluid's temperature must be maximum at the surface of the disk and minimum at locations far from the disk. Meaning the velocity and temperature profiles of the fluid must follow a trend similar to the one shown in Figure 1.1.

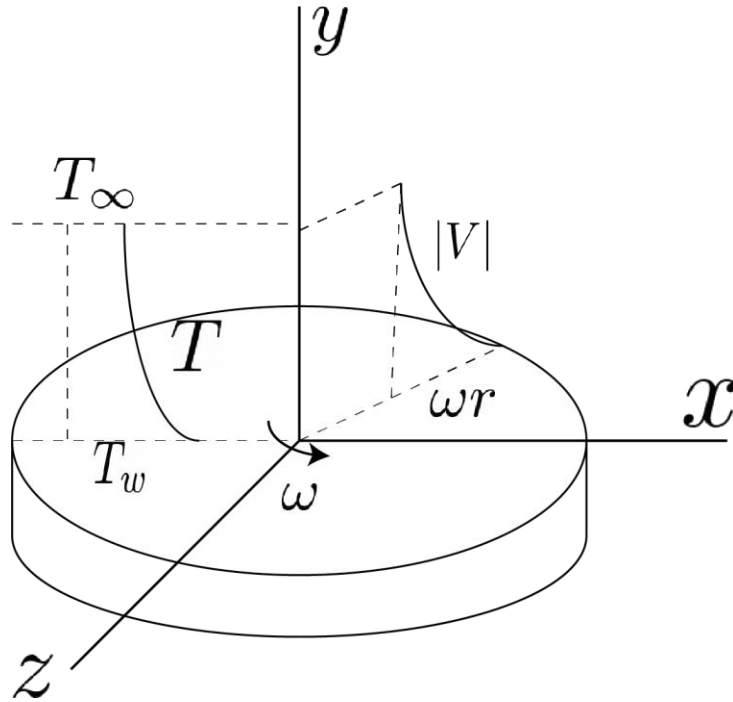


Figure 1.1: Velocity and temperature profiles over a rotating disk in still air

This characterizing behavior of a fluid interacting with a rotating disk provides a method to verify the model generated within the CFD software. The fluid within the CFD model must interact with the rotating disk and have the same behavior for both the temperature and velocity profile, as shown in Figure 1.1. For the case shown in Figure 1.1, the in-plane velocity,  $|V|$ , is found by using the two components of the velocity acting within the  $x$ - $z$  plane. Once obtained, the two components can be used to determine the magnitude of the in-plane velocity as follows

$$|V| = \sqrt{V_x^2 + V_z^2}. \quad 1.2$$

## 1.2 Validation of the Simulation by Comparing to Analytical Solutions

In this work, the results of the CFD software must compare and agree with published analytical results. An additional validation method for this work includes the creation of CFD simulation utilizing a secondary method to simulate the rotation of the disk. Analytical solutions for various forms of forced convective heat transfer are given in the form of relating the Reynolds number to the average Nusselt number (Eq 1.3). For a rotating body, a similar correlation is used. However, a rotational Reynolds number is used instead (Eq. 1.4).

$$Nu = C * Re^n. \quad 1.3$$

$$Nu_R = C_m * Re_\omega^n. \quad 1.4$$

For this work, the correlation for the average Nusselt number (Eq. 1.5) is based on the radius of the disk, average heat transfer coefficient, and the thermal conductivity of the fluid. The rotational Reynolds number (Eq. 1.6) is related to the angular velocity, the radius of the disk, and the kinematic viscosity of the fluid.

$$Nu_R = \frac{\bar{h}R}{k}. \quad 1.5$$

$$Re_\omega = \frac{\omega R^2}{\nu}. \quad 1.6$$

## 1.3 Thesis Objectives

In this work, the main objectives center around obtaining the value for the forced convective heat transfer coefficient of the fluid due to the rotation of the flat disk shown in Figure 1.2. The method employed in this work to obtain the convective heat transfer coefficient of the fluid is to utilize a CFD software. When using CFD software to solve a problem, a necessary step is to ensure that the problem is being represented correctly in the software. The verification can be done by comparing the temperature and velocity profiles within the simulation to the expected trends shown in Figure 1.1. Once the simulation is appropriately representing the physics of the problem, simulations can be conducted to obtain the value of the convective heat transfer coefficient for a

simple disk. The first method utilized to obtain the heat transfer coefficient is the global rotation method. The values obtained from the simulations must then be compared to the results reported in other works of literature. This step validates the results obtained from the CFD simulation. Once the results obtained from the simulation agree with published results, a second simulation with an entirely different procedure can be developed to strengthen the results of the CFD simulation for a smooth disk rotating in still air. The second method utilized is the local rotation (sliding) method. The development of a second procedure for the local rotation (sliding) method allows for a comparison of the two methods to better understand the CFD software and how rotation is simulated within the software.



Figure 1.2: Geometry for a rotating disk created in SolidWorks

The main objectives of this work are:

1. Verify the physics within the CFD software agrees with the expected results for the problem presented. The verification can be done by comparing the velocity and temperature profiles of the fluid within the simulation to the expected trends for both the temperature and velocity profiles.
2. Create a procedure using the global rotation method that users can follow to determine the heat transfer coefficient due to the rotation of the disk. The results from the procedure must agree with published results. Also, the procedure must use the information gathered from the verification process. Mainly, the procedure must outline the size of the computational domain.
3. Create a secondary procedure using the local rotation (sliding) method to ensure that the CFD software is displaying the correct results and that this secondary procedure also agrees with published results.

4. Compare the global rotation and local rotation (sliding) method for accuracy to provide insight as to which method is better for applications.
5. Expand the utilization of the best procedure to cover both low and high rotational speeds for a rotating disk while showcasing how the results compare with analytical solutions.

## **1.4 Thesis Organization**

The following listed items showcase the organization of the chapters presented. Additionally, a summary of each chapter is given.

### Chapter 1: Introduction

This chapter establishes the premise of the work. Also, the chapter aims to create a basic understanding of the physics within the problem.

### Chapter 2: Literature Review

Within this chapter, previous works relevant to the topic of heat transfer due to rotating bodies are summarized.

### Chapter 3: Problem Statement and Verification of the Model

This chapter aims to establish the main problem statement for the study and to showcase the steps taken when verifying the simulation created in the CFD software. The main items that were analyzed to verify the CFD model are the temperature and velocity profiles of the fluid surrounding the rotating disk.

### Chapter 4: Descriptions and Procedures for Global Rotation Method and Local Rotation (Sliding) Method

Within this chapter, the focus is on describing the two methods used to obtain values for the convective heat transfer coefficient. The methods being global rotation method and local rotation (sliding) method. A procedure for each method is given within the chapter.

#### Chapter 5: Comparison Between the Global Rotation and Local Rotation (Sliding) Methods

The results obtained from the two methods detailed in Chapter 4 are compared in this chapter. Additionally, within this chapter, the convergence for each method is shown when changing the size of the mesh used to discretize the computational domain.

#### Chapter 6: Testing for Full Range of Rotational Speeds

When creating the simulation in Chapter 4 and Chapter 5, the angular speed of the disk was low. For this chapter, the angular speed is increased to values that would fall within the transition and turbulent regions, as described by previous works of literature.

#### Chapter 7: Impact of Total Amount of Cells on Simulation Time and Expected Percent Difference

Within this chapter expected simulation times and percent differences are shown based on the regime tested and the total amount of cells present during the simulation.

#### Chapter 8: Conclusion

Within this chapter, the results of the work are summarized. Furthermore, this chapter outlines possible next steps to be considered to improve this work.

## 2. LITERATURE REVIEW

A review of the literature was done to understand the situation and the physics of the problem. The study of the literature allows for the development of a fundamental understanding of the problem that can be used to generate a CFD analysis. The CFD analysis, in turn, can be utilized to obtain results for the average convective heat transfer coefficient of a fluid due to a rotating disk. By generating a valid and verified CFD analysis, researchers can create scenarios within the computational domain that may be difficult to recreate in the laboratory. For a rotating disk, one difficulty is eliminating the effects of buoyancy due to the surrounding fluid at low rotational speeds. Within the CFD domain, the buoyancy effect of the fluid can be neglected, allowing the researchers to determine the heat transfer coefficient caused only by the rotation of the disk.

The reviewed literature detailed the methods used to determine the heat transfer coefficient of a rotating disk experimentally. Many experimental investigations utilized a design that allowed researchers to directly measure the heat input and the temperature of the disk under a steady-state condition. The design of the experimental apparatus allowed researchers to change the rotational speed of the disk freely. By using this apparatus, the researchers obtained heat transfer coefficient values for various rotational speeds. Once the heat transfer coefficient is determined, the Nusselt number correlations can be used to relate the average heat transfer coefficient to the rotational rate of the disk. Rotational Reynolds number is used to generate the Nusselt number correlations, with constant  $C_m$  and exponent  $n$ , as shown in Eq. 2.1. The rotational Reynolds number is based on the radius of the disk,  $R$ , the angular velocity of the disk,  $\omega$ , and the kinematic viscosity of the fluid,  $\nu$  (Eq. 2.2).

$$Nu_R = C_m * Re_\omega^n \quad 2.1$$

$$Re_\omega = \frac{\omega R^2}{\nu} \quad 2.2$$

A method used to determine the heat transfer coefficient due to a rotating disk experimentally was carried out in 1953 by Cobb and Saunders [1]. Cobb and Saunders utilized a double-sided, 18-inch diameter aluminum disk with a thickness of 3/8 inch attached to a 1-inch diameter shaft. The shaft

was attached to a motor that allowed the disk to rotate up to 2000 RPM. Thermocouples were used to measure the temperature near the edge and center of the disk. The measured temperatures were utilized to determine the heat transfer coefficient and the Nusselt number. By using the physical apparatus for experimentation with various rotational rates, Cobb and Saunders established correlations between the Nusselt number and the rotational Reynolds number for high rotational speeds.

During the experiments, Cobb and Saunders detailed sources of uncertainties associated with low rotational rates. While experimenting with low rotational rates, one of the primary sources that can cause uncertainties in physical experiments is the presence of the buoyancy of the fluid. This effect is lessened when experimenting within the turbulent regime. The expectation is that at high rotational speeds, the buoyancy effect from the fluids is negligible.

Cobb and Saunders, in the same study, experimentally obtained Nusselt number correlations for rotational Reynolds number above 240,000. This rotational regime is described as turbulent. They reported that the average Nusselt number is related to the rotational Reynolds number, with the constant,  $C_m$ , having a value of 0.015 and the exponent  $n=0.8$ .

In 1968, Dorfman [2] developed an analytical relation between the constant  $C_m$  and the Prandtl number of the fluid. The analytical solution was found using an integral method for a turbulent regime. When utilizing the analytical relation outlined by Dorfman, air at room temperature results in the constant  $C_m$  having a value of 0.01486 with the exponent  $n=0.8$  for a turbulent regime.

Later in 1973, Owen et al. [3] developed an experimental apparatus that allowed for a stream of air to interact with the rotating disk. The apparatus allowed them to study forced convective heat transfer due to the flow of air, convective heat transfer due to the rotation of the disk, or the heat transfer caused by the combination of the stream of air and the rotation of the disk. The apparatus was made using a 762 mm diameter disk attached to a shaft that was able to rotate up to a speed of 4000 RPM. Owen et al. carried out tests for various rotational speeds, and after obtaining the heat transfer coefficient, they obtained estimates for Nusselt number correlations. The value of the constant was  $C_m=0.0151$ , while the exponent value was  $n=0.8$ .

In 1975, Popiel and Boguslawski [4] experimentally determined the limits for laminar and turbulent regimes for a rotating disk. They estimated the limits for the laminar regime to fall between Reynolds number 10,000 to 195,000, while the turbulent regime is for Reynolds number above 250,000. They additionally obtained estimates for the Nusselt number correlation in the turbulent regime. They determined the constant to have a value of  $C_m=0.0145$  and the exponent to have a value of  $n=0.8$ . However, in 1981, Malik et al. [5] described the laminar regime to be for Reynolds number below 86,000 and the turbulent regime for Reynolds number above 210,000.

In 1997, Cardone et al. [6] presented a method to measure the heat transfer on rotating disks that utilized IR radiometers instead of thermocouples. The experimental apparatus included the use of a motor attached to a belt, and the motor caused the rotation of the disk. IR radiometers record the temperature across the surface of the disk as the experiment is conducted. During the experiment, a printed circuit is used to achieve a constant surface temperature. The IR radiometers are advantageous due to their spatial resolution and thermal sensitivity. These advantages make it possible to perform accurate measurements for low Reynolds numbers. By utilizing the IR radiometers, Cardone et al. determined the local heat transfer coefficient across the surface of the disk. The results for the local heat transfer coefficient were plotted as a contour plot on the surface of the disk. The contour plot showed the value of the local heat transfer coefficient and the location for that specific value on the surface of the disk.

In 2011, Latour et al. [7] created an experiment to investigate the effects of transverse air crossflow on the convective heat transfer of a rotating disk. In this study, a disk made of aluminum, with an inner radius of 20 mm, an outer radius of 80 mm, and a thickness of 2 mm. To be able to rotate the disk, a cylinder was passed through the inner radius of the disk and connected to an electrical motor that would be able to rotate at speeds up to 2000 RPM. The entire assembly was housed inside a 2-meter long wind tunnel. To measure the temperature distribution across the cylinder, an infrared camera, and radiant panel were used. High rotational speeds and high axial wind speeds were chosen to limit the uncertainty due to the buoyancy of the fluid. By utilizing the infrared camera, Latour et al. determined the local heat transfer coefficient across the surface of the disk. A contour plot was used to show the value and location of the local heat transfer coefficient across the surface of the disk.

Trinkl et al. [8], in 2011, carried out an experimental investigation using a rotating disk attached to a shaft that allowed the disk to rotate at high RPM. During this experiment, Trinkl et al. determined the heat transfer coefficient, which in turn allowed them to establish Nusselt number correlations. The constant had a value of  $C_m=0.015$ , and the exponent had a value of  $n=0.8$  for a turbulent flow, further validating results found by the previous researchers.

Weishce and Helcig [9], in 2016, experimentally obtained values for the heat transfer coefficient. The method used to determine the heat transfer coefficient included utilizing an apparatus that allowed a disk to rotate at various RPM, and thermocouples were attached to measure the temperature across the surface of the disk. By using the heat transfer coefficient, Weishce and Helcig plotted the Nusselt number versus the rotational Reynolds number and found the results to agree with a Nusselt number correlation that had an exponent value of  $n=0.5$  and a constant of  $C_m=0.3259$ . Additionally, Weishce and Helcig describe the fully turbulent regime to begin at rotational Reynolds number of  $10^6$ .

Shevchuk [10], in 2016, detailed the value for the leading coefficient,  $C_m$ , based on different Prandtl numbers for a laminar regime. The value for  $C_m$  was found analytically by solving the governing equations. For air, the constant has a value of  $C_m=0.3259$ , and the exponent was found to have a value of  $n=0.5$ . The values found analytically agree with the experiments conducted by previous researchers.

### 3. PROBLEM STATEMENT AND VERIFICATION OF MODEL

#### 3.1 Problem Statement

The main topic of this study is to obtain values for the forced convective heat transfer coefficient for the case of a rotating disk in a still fluid by using CFD software. The examined geometry is a simple disk with specified dimensions, shown in Figure 3.1. For the simulation, the disk rotates at various rates, and the buoyancy of the fluid is neglected by setting the gravitational acceleration within the CFD simulation to a value of zero. By having no gravity in the simulation, the type of convection studied in the CFD analysis is forced convection caused purely by the rotation of the disk.

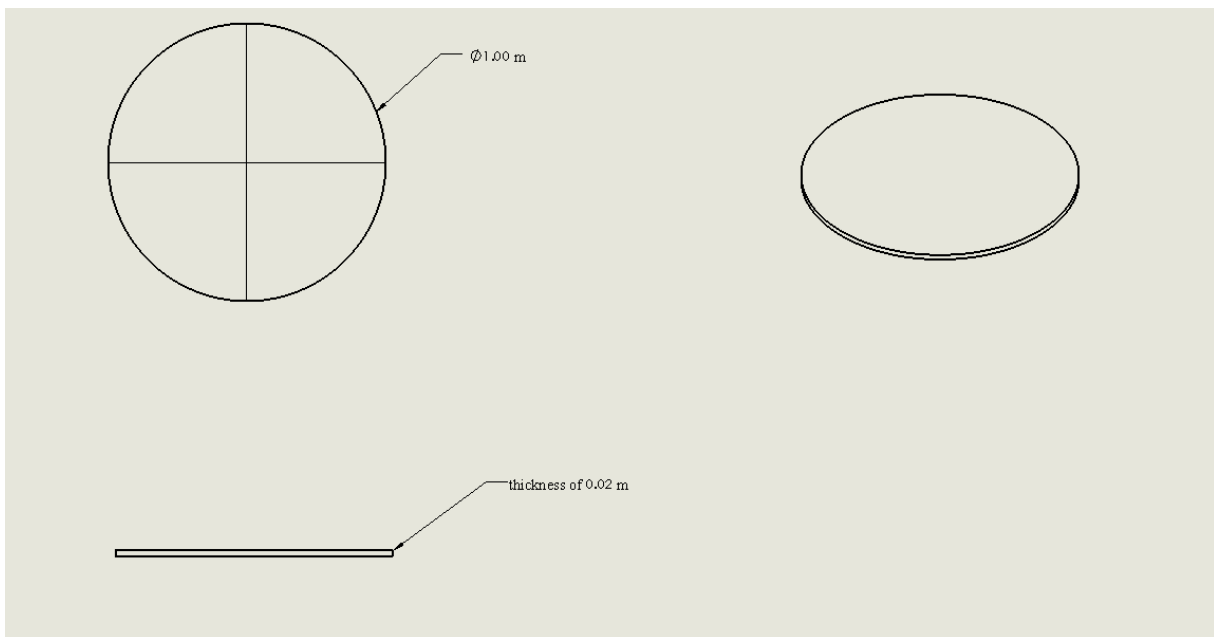


Figure 3.1: Dimensions of the disk created in SolidWorks

The first step when using SolidWorks' CFD is to generate the geometry that is to be studied. The generation of the geometry can be done in SolidWorks or imported from other software. In this study, the geometry of the disk was generated within SolidWorks. After creating the geometry, save the file within SolidWorks and initiate the CFD simulation. Illustrated in the next section is the full procedure for creating the disk geometry and launching SolidWorks' CFD software.

### 3.1.1 Mathematical Modeling

Igor V. Shevchek in 2016 showed the mathematical model for the physical problem. Shevchek began by considering the continuity, momentum and heat transfer differential equations in rectangular coordinates and then converted to cylindrical coordinates. Once in cylindrical coordinates the continuity, momentum, and heat transfer equations were simplified to represent a disk rotating in a still fluid. The following are the differential equations of the boundary layer

$$v_r \frac{\partial v_r}{\partial r} - \frac{v_\phi^2}{r} + v_z \frac{\partial v_r}{\partial z} = -\frac{1}{\rho} \frac{\partial p}{\partial r} + \frac{1}{\rho} \frac{\partial}{\partial z} \left( \mu \frac{\partial v_r}{\partial z} - \rho \overline{v'_r v'_z} \right), \quad 3.1$$

$$v_r \frac{\partial v_\phi}{\partial r} + \frac{v_r v_\phi}{r} + v_z \frac{\partial v_\phi}{\partial z} = \frac{1}{\rho} \frac{\partial}{\partial z} \left( \mu \frac{\partial v_\phi}{\partial z} - \rho \overline{v'_\phi v'_z} \right), \quad 3.2$$

$$\frac{1}{\rho} \frac{\partial p}{\partial z} = 0, \quad 3.3$$

$$\frac{\partial T}{\partial t} + v_r \frac{\partial T}{\partial r} + v_z \frac{\partial T}{\partial z} = -\frac{1}{\rho c_p} \frac{\partial}{\partial z} \left( \lambda \frac{\partial T}{\partial z} - \rho c_p \overline{T' v'_z} \right). \quad 3.4$$

The following assumptions correspond to these governing equations for this problem:

1. Velocity components  $v_r$  and  $v_\phi$  are an order of magnitude larger than the  $v_z$  velocity component
2. Velocity and temperature vary in the  $z$ -direction much more significantly than they do in the  $r$ -direction
3. Variation of the static pressure,  $p$ , in the  $z$ -direction is negligible
4. The turbulence parameters  $\overline{v'_r}$ ,  $\overline{v'_\phi}$ ,  $\overline{v'_z}$ , and  $\overline{T'}$  are only neglected when considering laminar flow
5. The heat transfer only occurs on the top surface of the disk. Indicating that the side and bottom of the disk are adiabatic

The boundary condition for this problem include:

1.  $V|_{z=0} = \omega r$
2.  $V|_{z=\infty} = 0$
3.  $T|_{z=0} = T_w$
4.  $T|_{z=\infty} = T_\infty$

### 3.1.2 Detailed Procedure to Create a Disk in SolidWorks

1. Open SolidWorks and edit the document units to be in SI units. Figure 3.2 shows the quick access for changing the document units.

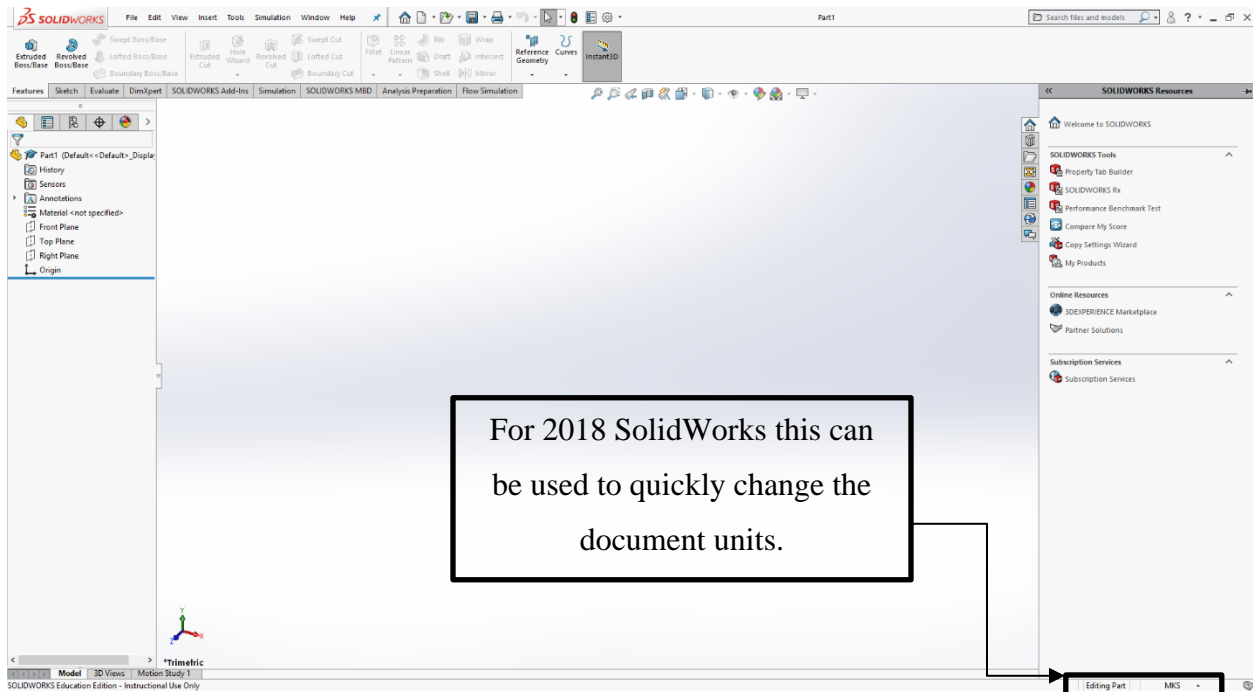


Figure 3.2: How to quickly change the document units once SolidWorks is opened

2. Use the top plane as the initial sketch plane shown in Figure 3.3. Using the top plane only impacts the orientation of the disk if and only if gravity is on during the CFD analysis. Generally, SolidWorks has a default setting for gravity to be in the negative y-direction, but this setting can be changed to the user's preference when initializing the CFD analysis and, as such, the initial plane used for the initial sketch does not impact the CFD analysis.

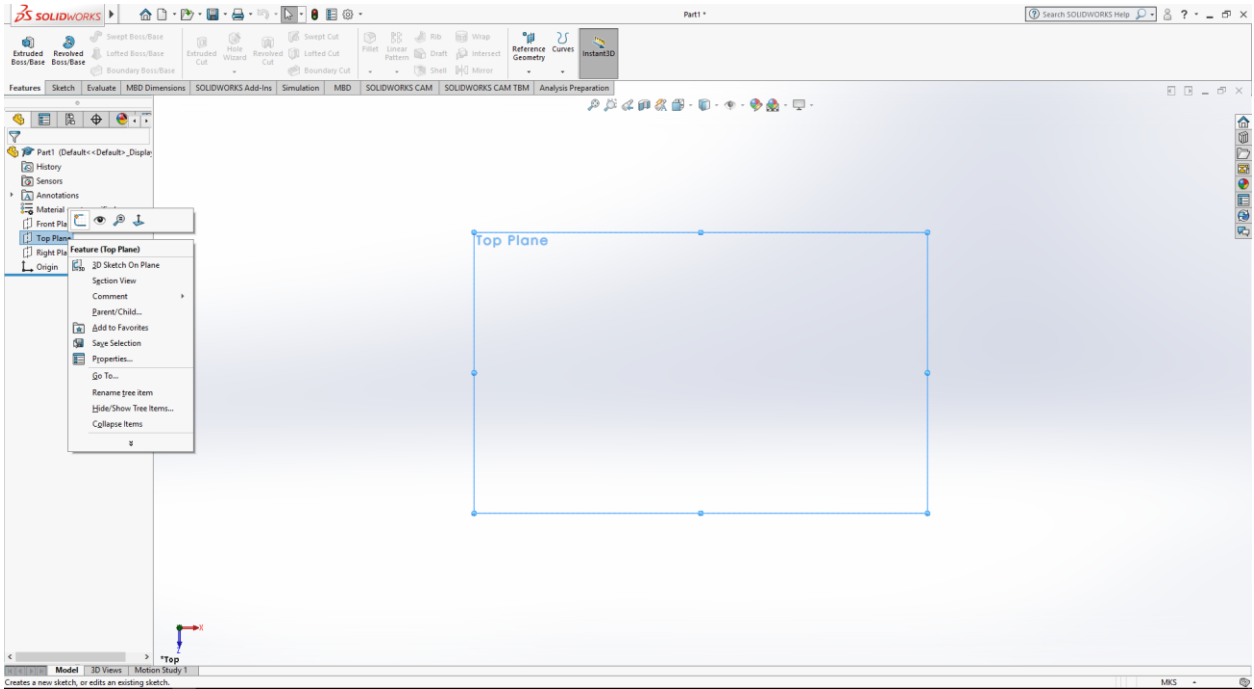


Figure 3.3: Begin the sketch on the top plane to create the disk geometry within SolidWorks

3. Create a circle with the center at the origin and with a diameter of 1 meter, as shown in Figure 3.4.

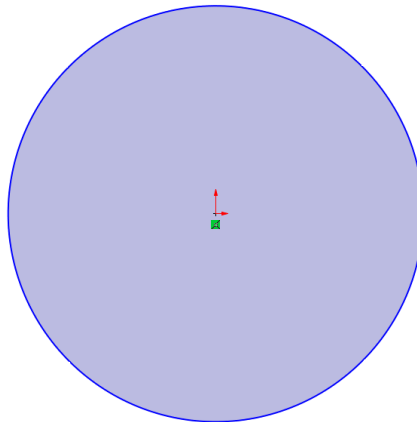


Figure 3.4: Basic geometry of the disk with the center at the origin and diameter of 1 m

4. Extrude the circle using the midplane option to a thickness of 20 mm. The midplane option keeps the geometry of the disk symmetric about the origin. **Error! Reference source not found.** shows the final geometry of the disk.

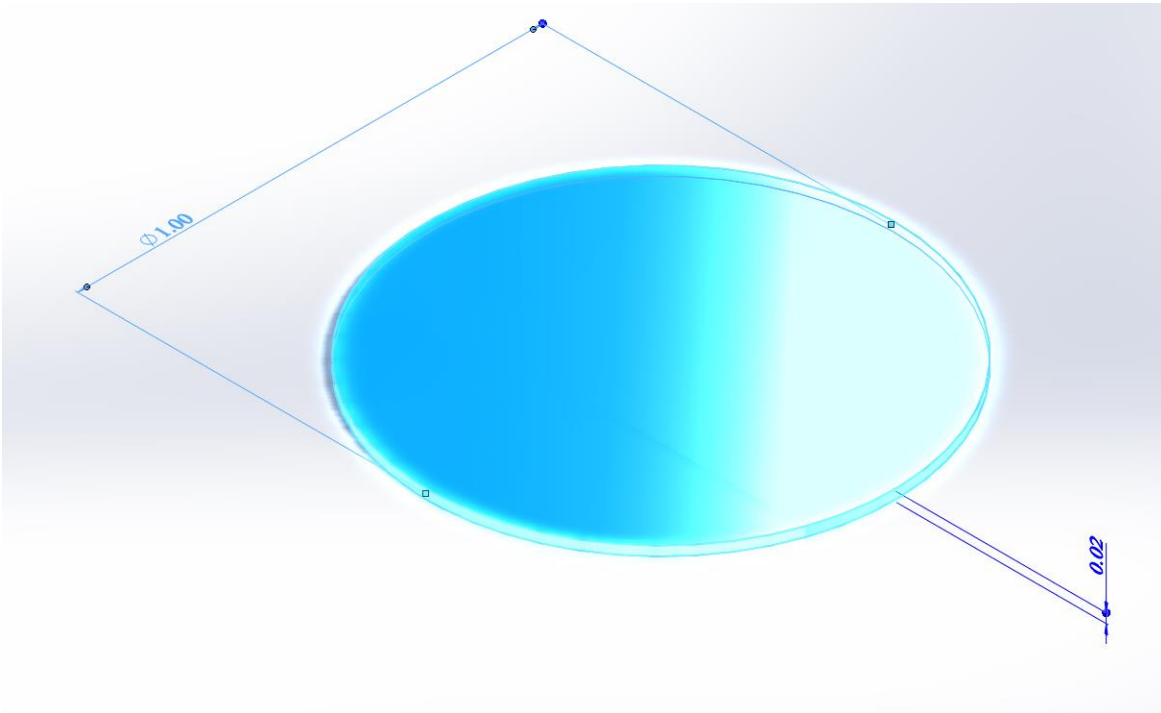


Figure 3.5: Final geometry of the disk including the dimensions all in meters

### 3.2 Verification of the Model

When creating a model that represents a physical system, an appropriate step is to verify that the model generated is correctly built. A viable option when verifying the CFD analysis of a rotating disk at a constant temperature is to check the temperature and velocity profiles of the fluid during the CFD simulation. When the rotating disk is in stationary fluid, the temperature profile needs to show that the disk and fluid have the same temperature at the surface of the disk. The velocity profile of the fluid needs to show that the velocity is maximum at the surface of the disk and approaches a value of zero at distances far from the disk.

### 3.2.1 Velocity and Temperature Profiles

For the temperature and velocity profiles, the maximum value is near the surface of the disk, and the minimum value is at locations far away from the surface. The velocity profile is analyzed using the in-plane velocity, the velocity parallel to the x-z plane. The magnitude of the in-plane velocity across the surface of the disk can be determined using the x and z coordinates of the fluid's velocity.

Items that are checked to verify the CFD software physics include:

- At any specific radial position, the in-plane velocity is independent of the coordinates used. For example, the x-z coordinates  $x=0.25$  m, and  $z=0.00$  m has the same velocity profile as  $x=0.00$  m, and  $z=0.25$  m.
- The temperature and velocity profiles must range from maximum values at the surface of the disk to minimum values far from the surface of the disk.
- The items used to characterize the temperature and velocity profile is the dimensionless temperature (Eq. 3.5) and the dimensionless velocity (Eq. 3.6):

$$\theta^* = \frac{T - T_\infty}{T_w - T_\infty} \quad 3.5$$

$$V^* = \frac{|V|}{\omega r} \quad 3.6$$

Figure 3.6 shows the general trend found when plotting either the velocity profile or the temperature profile of the fluid. Due to the majority of the difference occurring below heights of 0.3 m, all plots after Figure 3.6 show an amplified view of the results.

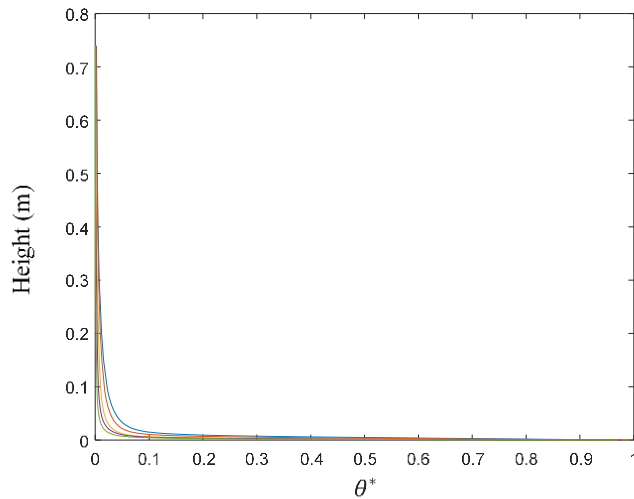


Figure 3.6: Plot showing the full range for a temperature profile

Observations seen from the entire trend shown in Figure 3.6 are that the maximum value for the temperature profile is near the surface of the disk. The minimum value is found at distances far from the surface of the disk, roughly around one meter. This general trend is found similarly for all other velocity and temperature profiles.

The first item analyzed is the independence of the velocity profile due to the x-z coordinates. The independence of the velocity profile was analyzed using the capabilities within SolidWorks' Fluid Flow simulation to probe anywhere within the computational domain of the CFD simulation for various variables. Table 3.1 summarizes the coordinates for each location. At each location, the velocity profile is captured, and Figure 3.7 shows the dimensionless velocity at each location. Each location has the same radial distance from the center of the disk but different x-z coordinates. Due to having the same radial position, the velocity profile is expected to be the same.

Table 3.1: Summary of the locations used to verify the CFD simulation

	<b>X Coordinate (m)</b>	<b>Z Coordinate (m)</b>
<b>Location 1</b>	0.25	0.00
<b>Location 2</b>	-0.25	0.00
<b>Location 3</b>	0.00	0.25
<b>Location 4</b>	0.00	-0.25

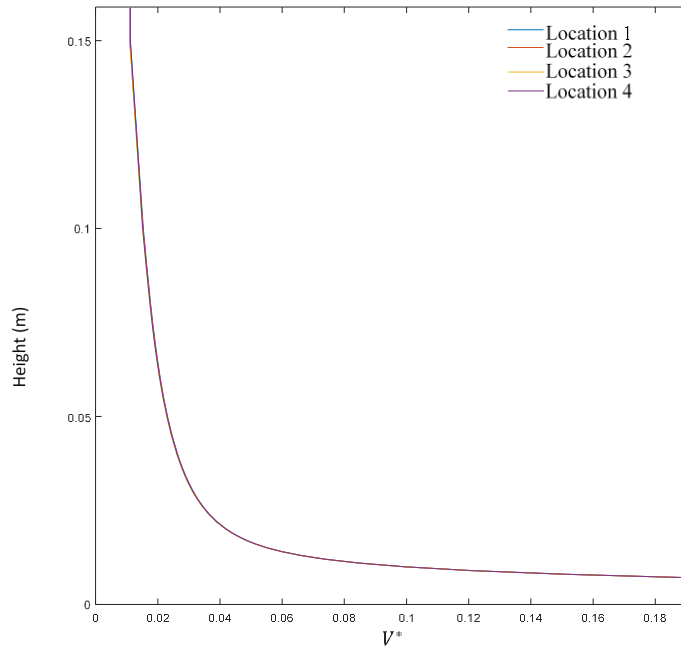


Figure 3.7: Dimensionless velocity profile at various locations along the surface of the disk

Figure 3.7 shows that the dimensionless velocity profile is the same at all locations tested. By having the same results for the dimensionless velocity, the in-plane velocity must also be the same at each of the locations. Figure 3.7 verifies that in-plane velocity is indeed independent of the coordinates used for a specified radial position.

Additional items to check are the profile differences due to the rotational rate, and the profile differences due to the radial position. Figure 3.8 shows the dimensionless temperature profile as the rotational rate of the disk is changing. Figure 3.9 shows the effects the radial position has on the dimensionless temperature profile. For both figures, the maximum value is near the surface of the disk, and the minimum value is at a distance far from the surface.

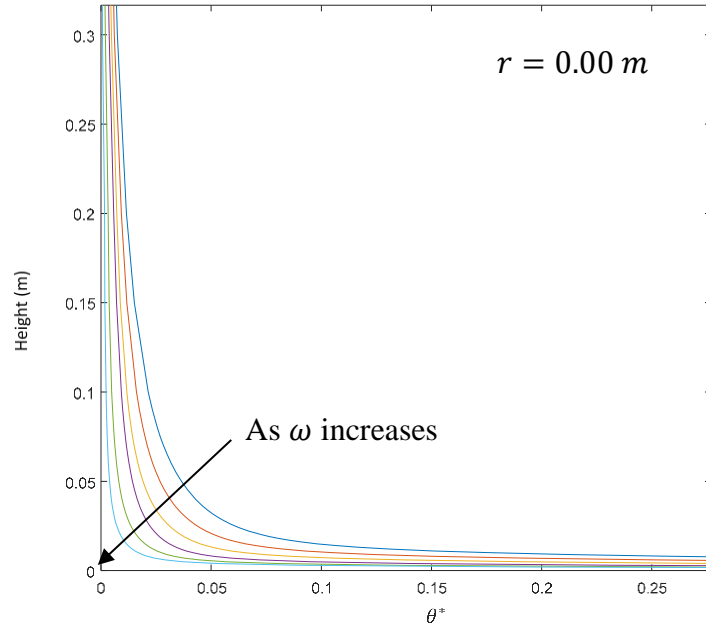


Figure 3.8: Dimensionless temperature profile plot for various rotational rates

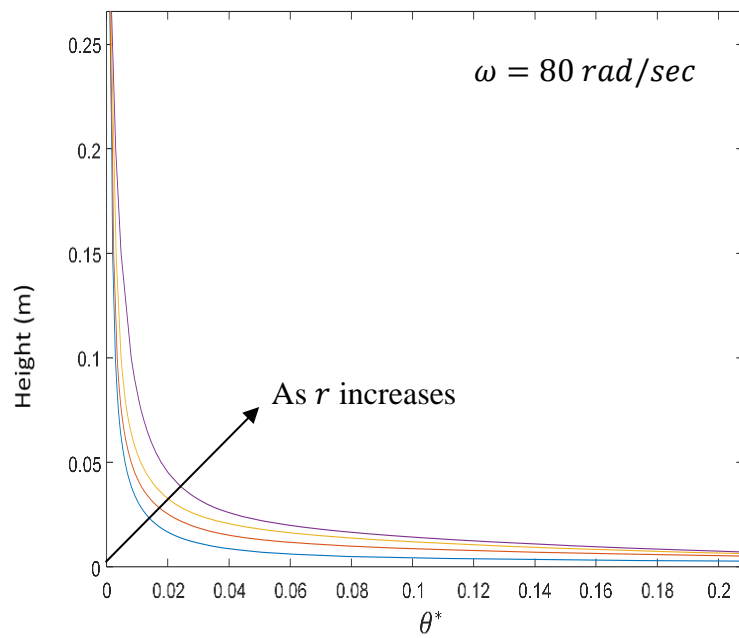


Figure 3.9: Dimensionless temperature profile plot to show the effects as radial position changes

A trend appears in Figure 3.8, showing that as the rotational rate increases, the faster the temperature profile changes from a maximum value near the surface of the disk to a minimum value at distances far from the surface of the disk. At the height of 0.05 meters off of the surface of the disk, the fastest rotation shows that the dimensionless temperature is around 1% off of the value of the ambient temperature. In contrast, the slowest rotation is at around 4% of the ambient temperature at the height of 0.05 meters.

Figure 3.9 shows a trend that as the radial position increases, the slower the temperature profile changes from a maximum value near the surface of the disk to a minimum value at distances far from the surface of the disk. At the height of 0.05 meters off of the surface of the disk, positions closer to the center of the disk show that the dimensionless temperature is around 1% off of the value of the ambient temperature. In contrast, the farthest radial position is at around 2% of the ambient temperature at the height of 0.05 meters.

Figure 3.10 shows the dimensionless velocity profile as the rotational rate of the disk is changing. Figure 3.11 shows the effects the radial position has on the dimensionless velocity profile. For both figures, the maximum value is near the surface of the disk, and the minimum value is at a distance far from the surface of the disk.

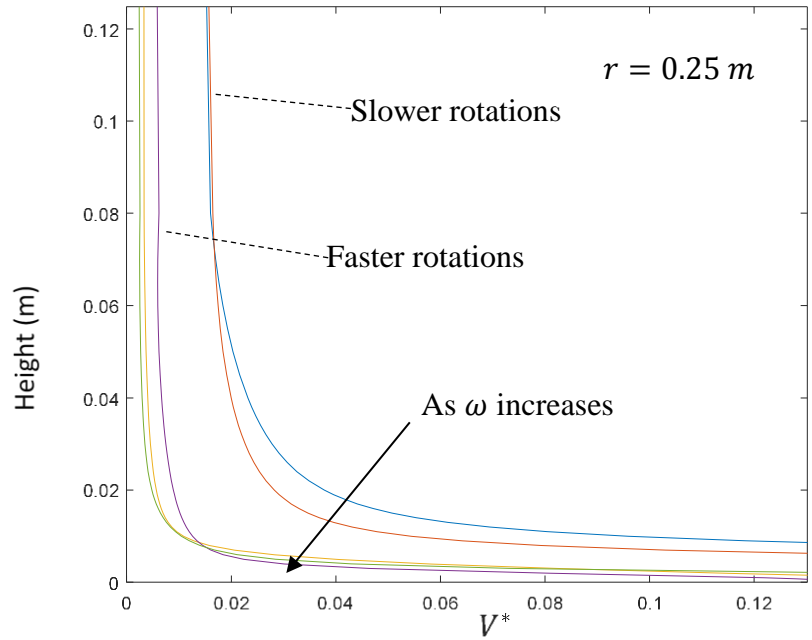


Figure 3.10: Dimensionless velocity profile plot for various rotational rates

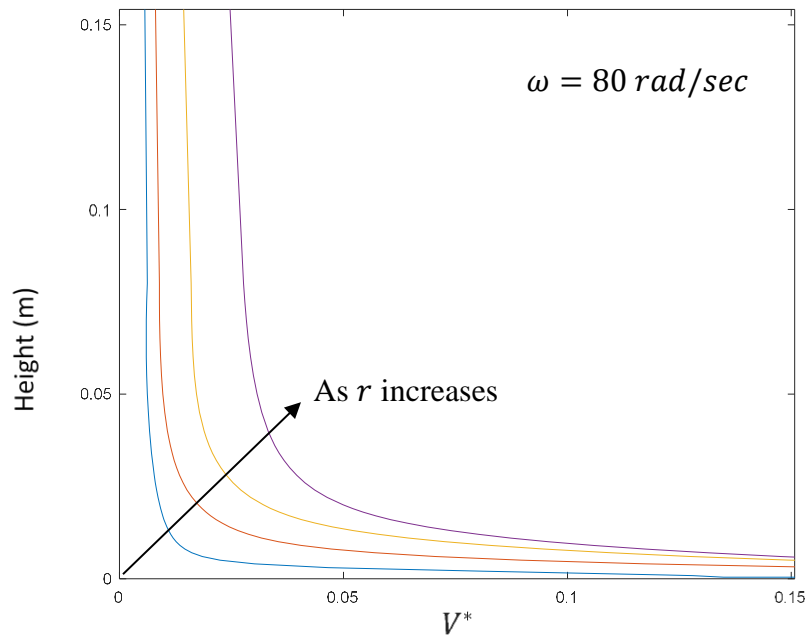


Figure 3.11: Dimensionless velocity profile plot to show the effects as radial position changes

In Figure 3.10, a clear distinction appears, the slow rotations are in one group, while the fast rotations are in another group. This observation shows that SolidWorks simulation is capturing behaviors that indicate the existence of different flow regimes. In general, the faster the rotation, the quicker the dimensionless velocity profile approached the maximum value near the surface of the disk and the minimum value at a distance far from the surface of the disk.

Figure 3.11 shows a trend that as the radial position increases, the slower the dimensionless velocity profile changes from a maximum value near the surface of the disk to a minimum value at distances far from the surface of the disk. At the height of 0.05 meters from the surface of the disk, positions closer to the center of the disk show the dimensionless velocity is around 1% the value of the ambient velocity of the fluid. The ambient fluid is still air. In contrast, the farthest radial position is at around 4% of the ambient velocity of the fluid at a height of 0.05 meters.

The height of the computational domain can be estimated from the results of both the dimensionless temperature profile and the dimensionless velocity profile. All profiles captured showed that at heights near 1 meter off of the surface of the disk, the values are near the ambient condition, and no changes occur above this height, which means that the minimum height of the computational domain must be 1 meter.

To ensure no issues arise when using the CFD software when acquiring results for the heat transfer coefficient, the domain size must be larger 1 meter. Any smaller can cause inaccuracies within the CFD analysis due to disruptions of the temperature and velocity profiles.

## 4. DESCRIPTIONS AND PROCEDURES FOR GLOBAL ROTATION METHOD AND LOCAL ROTATION (SLIDING) METHOD

When generating the CFD analysis for a rotating disk, a critical setting that the user must define is the method used to simulate the rotation of the disk. Within SolidWorks, there are three methods to simulate rotation on a body within the program. The methods are broken down into two categories those being either global or local rotation. Local rotation is further broken down into the sliding method and the averaging method. For this study, the two methods used are the global rotation method and the local rotation (sliding) method.

### 4.1 Global Rotation Method: Description

The global rotation method within SolidWorks takes into consideration the angular velocity that was defined. From here, the speed for each particle within the domain is determined as the fluid interacts with the disk. However, SolidWorks does not merely determine the velocity of the point; instead, SolidWorks, as outlined by [11], calculates the mass-distributed force (Eq. 4.1).

$$S_i^{rotation} = -2e_{ijk}\omega\rho u_k + \rho\omega^2 r_i. \quad 4.1$$

This relation allows SolidWorks to work with forces directly. By working with the forces interacting with the fluid, SolidWorks can determine various physical quantities, including the velocity profile of the fluid and the heat transfer coefficient of the fluid. The following section details the procedure utilized to create a global rotation simulation.

#### 4.1.1 Detailed Procedure for Global Rotation Method

1. Generate the geometry with any 3D modeling software and open the geometry in SolidWorks. Once the geometry is open in SolidWorks, save the geometry and open the CFD software wizard in SolidWorks. The wizard starts with the project name section shown in Figure 4.1.

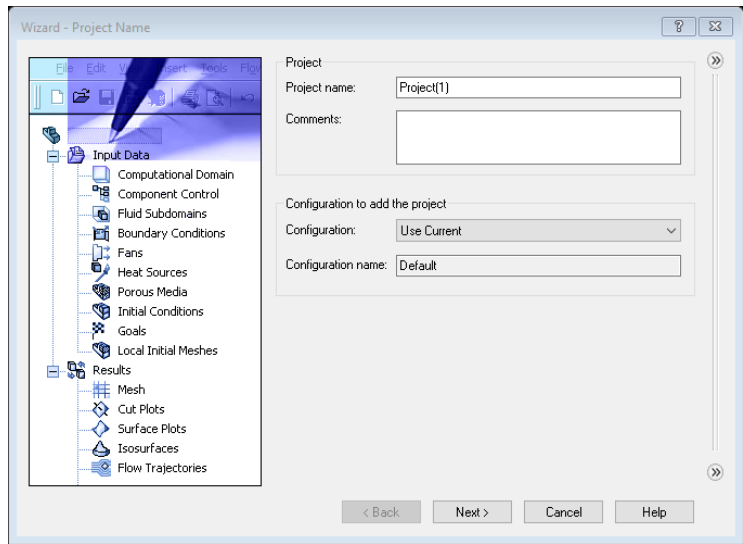


Figure 4.1: Project wizard first pop-up screen used to name the CFD simulation file

2. The units selected were SI, as shown in Figure 4.2.

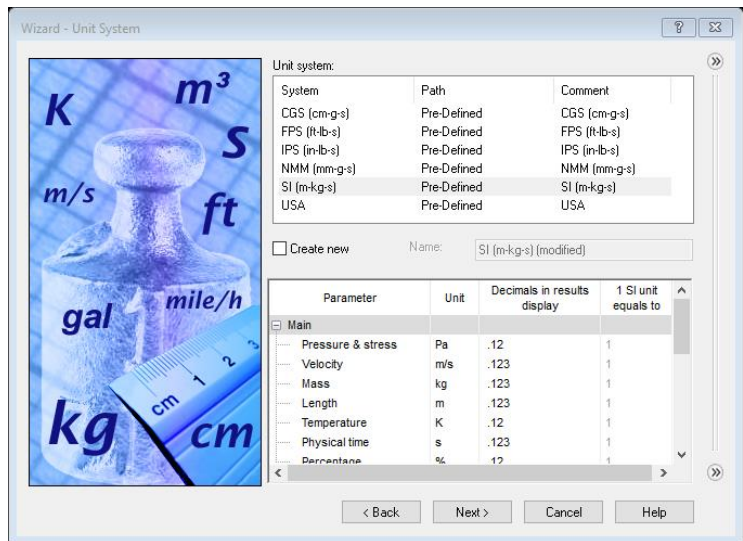


Figure 4.2: Units selected for the CFD simulation

3. Select the type of flow for the simulation and the settings used within the simulation. For this work, the simulation type is external, time-dependent is selected, rotation is selected, and the method of rotation is set to global rotation about the y-axis, shown below in Figure 4.3.

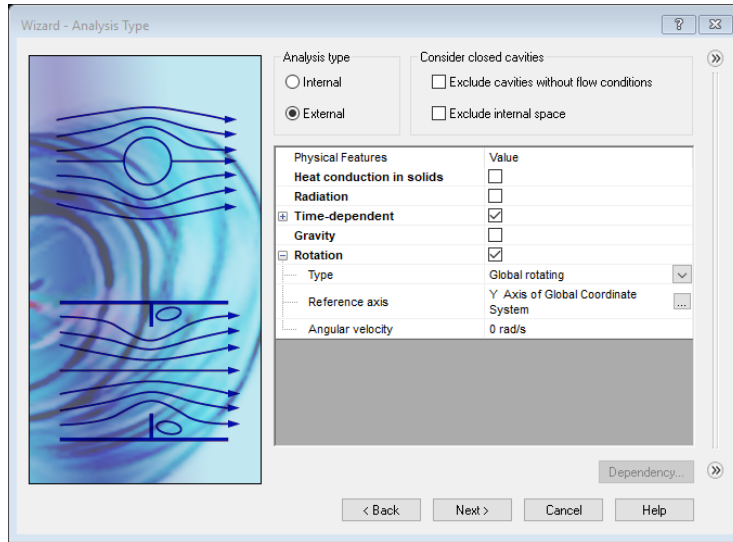


Figure 4.3: Settings for the CFD simulation

4. Select the fluid type, and set the temperature for the solid to a value of 393.2 K. The fluid is chosen as shown in Figure 4.4, and the temperature of the solid is shown in Figure 4.5.

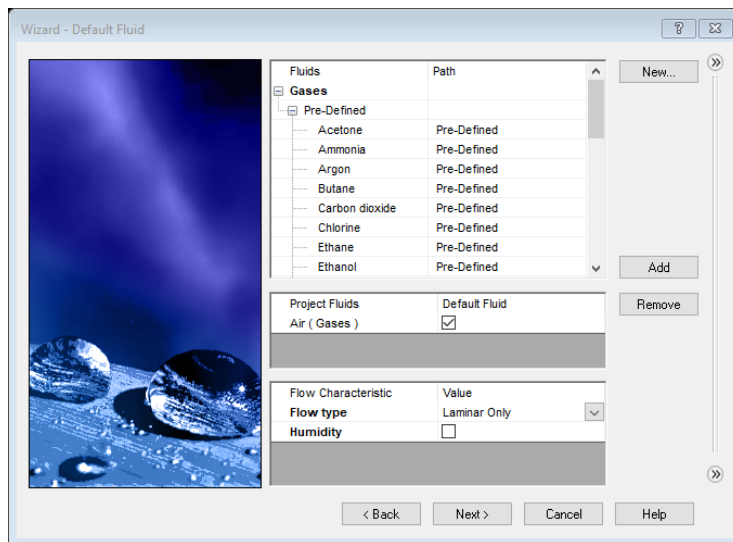


Figure 4.4: Fluid selected for the initial CFD simulation

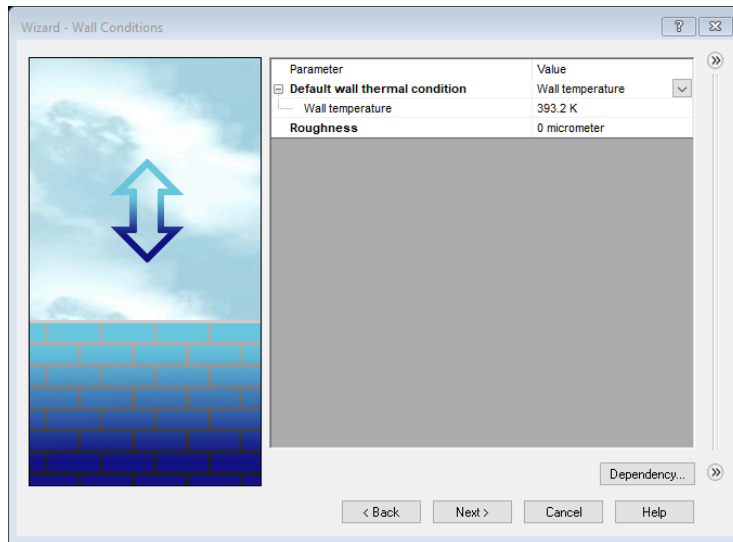


Figure 4.5: Temperature of the disk within the CFD simulation

5. Select the initial and ambient conditions. Figure 4.6 shows the settings used.

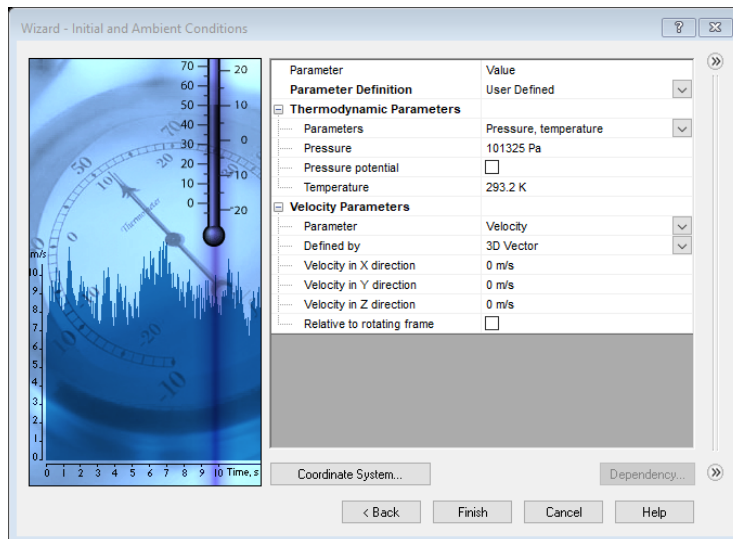
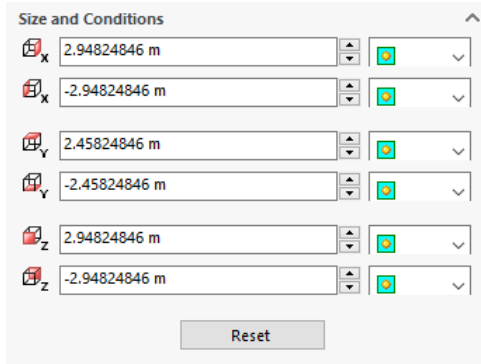
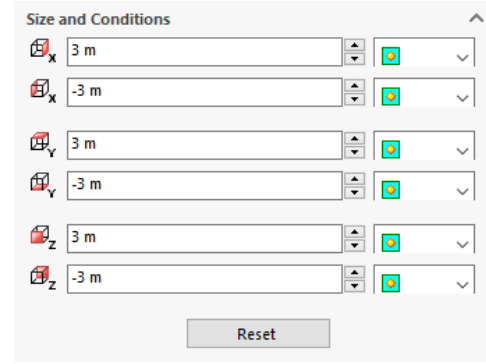


Figure 4.6: Initial and ambient conditions used during the global rotation method

6. Once the simulation opens in SolidWorks, change the domain size to the appropriate size. For this simulation, the domain size is three meters. The domain size is large enough not to disturb the velocity and temperature profiles. This change is highlighted in Figure 4.7. Figure 4.7 (a) is the default size created by SolidWorks, while Figure 4.7 (b) is the user-generated computational domain and conditions.



(a)



(b)

Figure 4.7: The computational size and conditions used within the CFD analysis and simulation

7. Add a local mesh to the surface of the disk. The local mesh allows the user to better capture the behavior of the fluid close to the disk. Figure 4.8 shows the selected surfaces of the disk where the local mesh was added to, and Figure 4.9 shows the settings for the local mesh.

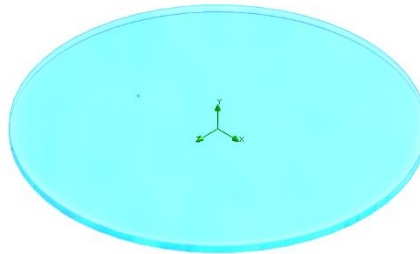


Figure 4.8: Selected surfaces of the disk which have the local mesh generated

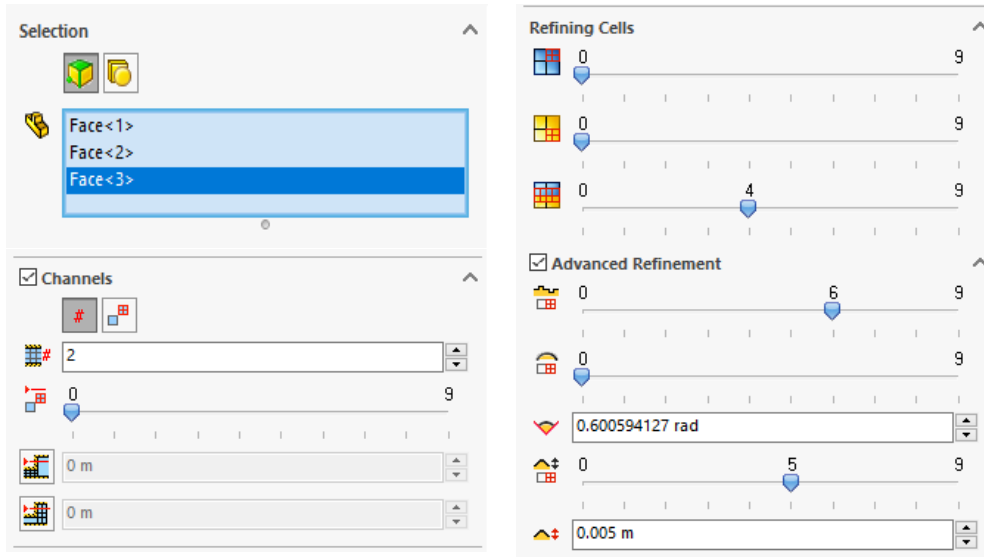


Figure 4.9: Setting of the local mesh

8. Add a boundary condition onto the bottom and side of the disk. The boundary condition selected makes the bottom and the side of the disk adiabatic. The boundary condition is shown in Figure 4.10.

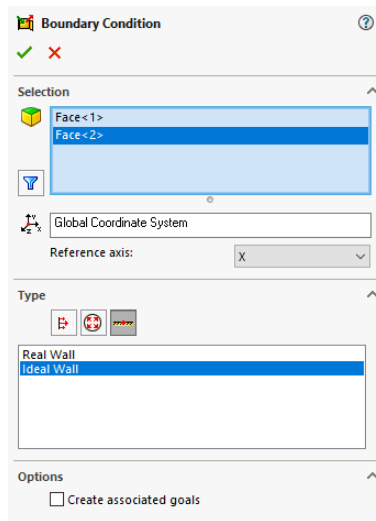


Figure 4.10: Adiabatic boundary conditions for the bottom and side of the disk

9. The primary variable that is analyzed is the average heat transfer coefficient. The heat transfer coefficient can either be chosen as a global goal that considers the behavior of the entire domain or by selected surface goals.

10. Keep the global mesh size as the default setting. This setting can be changed to improve the accuracy of the domain discretization.
11. Set the convergence percentage of the heat transfer coefficients (global and surface) to 3% and run the simulation until the values for the heat transfer coefficient have converged. The convergence parameter is used as the maximum acceptable percent difference. Predictions with a percent difference above 3% are deemed unacceptable, and predictions with percent differences below 3% are deemed acceptable.
12. Obtain the results from the CFD simulation and compare to expected results from analytical solutions, or other correlations available in the literature.

## **4.2 Local Rotation (Sliding) Method: Description**

The second method within SolidWorks to simulate rotation is local rotation. Local rotation is further broken down into two methods those being an averaging method and a sliding method. Both methods require a secondary body, not the solid under analysis, to be described as the rotating object. Instead of considering the entire domain as rotating about an axis, the local rotation (sliding) method describes a small section of the entire domain to be rotating. According to the SolidWorks technical reference [11], the difference between the sliding method and the averaging method is the interaction between the rotating body and the fluid. If the interaction between the rotating body and the fluid is significant to the study being conducted, the sliding method is recommended. However, the sliding method is more demanding computationally than the averaging method due to the sliding method assuming an unsteady flow field and requiring an unsteady numerical solution. The following section outlines the procedure to generate a local rotating region using the sliding method.

### **4.2.1 Detailed Procedure for Local Rotation (Sliding) Method**

1. Generate a disk similar to the one outlined in Chapter 3, where the dimensions are 1 meter in diameter and 20 millimeters in thickness.
2. A secondary body must now be generated that surrounds the disk and is tall enough not to disrupt the temperature and velocity profiles of the fluid. The secondary body can be a large cylinder made such that the bottom of the cylinder is 20 mm below the bottom of the

disk, and the height of the cylinder is 2 meters. The diameter of the secondary body must be slightly larger than the initial disk generated. As such, a diameter of 1.05 meters is used. The 2 meters is tall enough not to disturb the velocity profile or temperature profile. Figure 4.11 shows the dimensions of the cylinder generated.

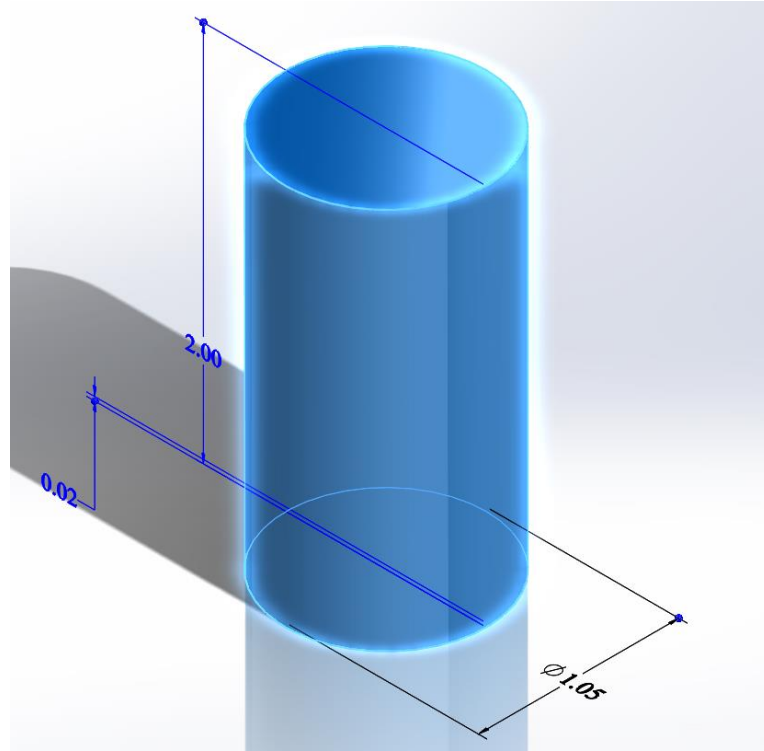
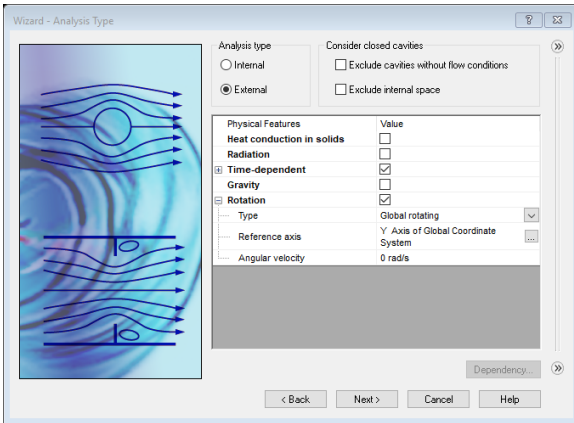
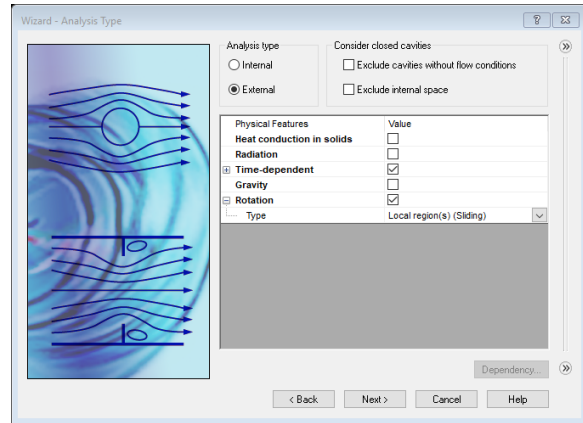


Figure 4.11: Secondary body generated to create the local rotating domain

3. Change the transparency so that the secondary body is transparent, allowing the user to see the main body being analyzed.
4. Initializing the CFD software is similar to steps 1 and 2 found in the procedure for the global rotation method, where the CFD analysis is named, and the units are selected.
5. When the flow type and the physical features are selected instead of choosing global rotation, the user selects '*Local Region(s) (Sliding)*' as shown in Figure 4.12 below. Figure 4.12 (a) is the global rotation settings used, while Figure 4.12 (b) is the sliding method settings.



(a)



(b)

Figure 4.12: Settings for global rotation method and the local rotation (sliding) method

6. Select the working fluid and set all other parameters similar to the ones found in the procedure for the global rotation method.
7. Set the domain to be a cube with a length of 3 meters.
8. Set the appropriate boundary conditions onto the disk and generate a local mesh around the disk.
9. Keep the default settings for the global mesh generated.
10. Set the convergence to 3%. The convergence parameter is used as the maximum acceptable percent difference. Predications with a percent difference above 3% are deemed unacceptable, and predications with percent differences below 3% are deemed acceptable.
11. However, before starting the simulation, the secondary body must have an assigned angular velocity shown in Figure 4.13.

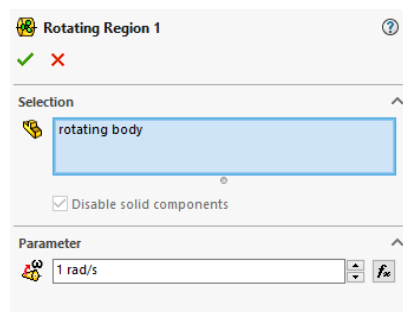


Figure 4.13: Angular velocity assigned to the secondary body generated

To accurately compare the results between the two rotating methods, all settings must be the same. The settings that can cause significant discrepancies are the mesh settings. However, this does not guarantee the two methods generate the same number of cells within the domain. The difference in cell number is due to the local region, placing more cells around the secondary body in an attempt to capture the rotation adequately. All mesh settings are set to the same values when for both methods to limit the discrepancies.

## 5. COMPARISON BETWEEN THE GLOBAL ROTATION AND LOCAL ROTATION (SLIDING) METHODS

By using the same mesh settings in each simulation, a direct comparison between the two methods can be made. To observe the convergence of the results, the only setting that was varied was the level of the initial mesh in the 'Global Mesh Settings.' The following figures show the settings used for both the global and local mesh. The local mesh was placed on the surface of the disk, similar to the disk made in Chapter 4. In Figure 5.1, a box is around the level of the initial mesh setting. Figure 5.2 shows all the settings used for the local mesh.

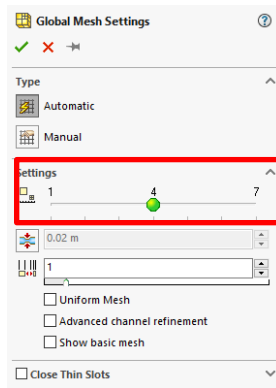


Figure 5.1: Global mesh settings used during each set of simulations

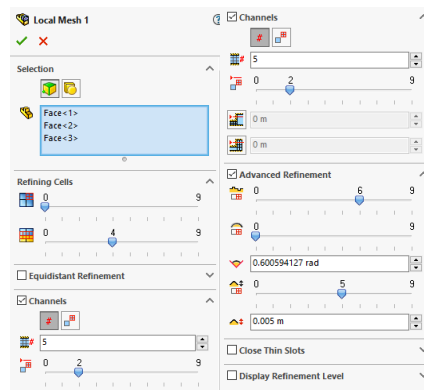


Figure 5.2: Local mesh settings used during each set of simulations

Various simulations were conducted by using a parametric study for both the global rotation method and the local rotation (sliding) method. During a parametric study, the user must define

both the input variables that can be monitored and changed if desired and define the output parameters. For both simulations, the input variables were the angular velocity and the level of the initial mesh. Table 5.1 shows the values used in these settings. The only output parameter that was defined is the heat transfer coefficient.

Table 5.1: Parametric study input variables for both methods

<b>Level of the initial mesh</b>	1, 2, 3, 4
<b>Angular velocity (rad/sec)</b>	0.5, 1.0, 2.0, 3.0, 4.0

For this comparison, the rotational velocity of the disk is kept low and within the laminar regime. The results are organized based on the level of the initial mesh. Each plot and table generated corresponds to the level of the initial mesh. The plots show the rotational Reynolds number on the x-axis while the y-axis is the Nusselt number. The tables show the results for the heat transfer coefficient using the Nusselt number correlations, the results obtained from the CFD simulation for both methods, and their respective percent differences. The Nusselt number correlation, as outlined by Weishce and Helcig [9], is

$$Nu_R = \frac{\bar{h}R}{k} = 0.3259 * Re_\omega^{0.5}. \quad 5.1$$

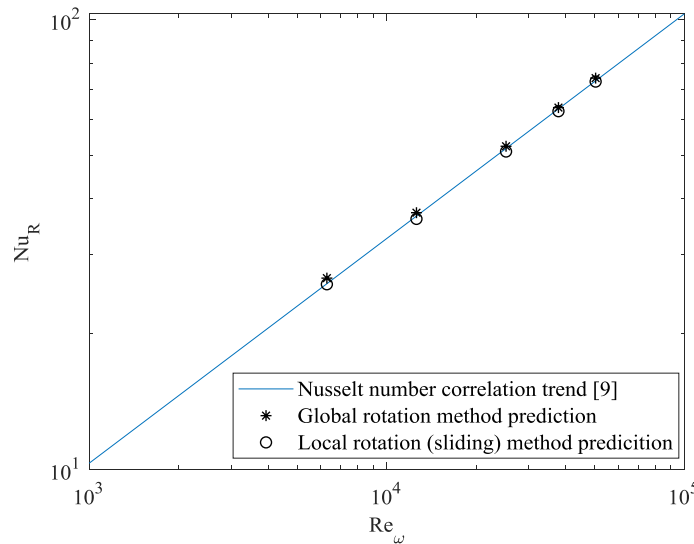


Figure 5.3: Results obtained for the both methods using a level of the initial mesh size of 1

Table 5.2: Summary of the results for both methods when the initial mesh level is set at 1

<b>Angular velocity (rad/sec)</b>	<b>Rotational Reynolds number</b>	<b>Expected result from [9] (W/m<sup>2</sup>-K)</b>	<b>Global rotation results (W/m<sup>2</sup>-K)</b>	<b>Percent difference (%)</b>	<b>Local rotation results (W/m<sup>2</sup>-K)</b>	<b>Percent difference (%)</b>
<b>0.5</b>	6.29E+03	1.5265	1.5709	0.72	1.5222	-0.07
<b>1.0</b>	1.26E+04	2.1588	2.1966	0.43	2.1279	-0.36
<b>2.0</b>	2.52E+04	3.0530	3.0875	0.28	3.0053	-0.39
<b>3.0</b>	3.78E+04	3.7391	3.7639	0.16	3.6947	-0.30
<b>4.0</b>	5.04E+04	4.3176	4.3770	0.34	4.3005	-0.10

Figure 5.3 and Table 5.2 summarize the results obtained for both methods for a level of the initial mesh size of 1. What can be observed from the plot is that both the local and global rotation methods obtain values that agree with the values predicted using the Nusselt number correlation outlined by Weishce and Helcig [9].

The local rotation (sliding) method underestimates the value of the heat transfer coefficient. The underestimation can be seen in both Figure 5.3 and Table 5.2. In Figure 5.3, the Nusselt number values fall slightly below the trendline for a laminar regime. In Table 5.2, the percent differences associated with the local rotation (sliding) method are negative, indicating that the value is lower than predicted. However, when looking at the absolute value of the percent differences, the local rotation (sliding) method has a smaller difference in three of the five trials. The lower percent differences in three of the five trials indicate that for a level of the initial mesh size of 1, the local rotation (sliding) method was more accurate.

In contrast, the global rotation method is overestimating the value of the heat transfer coefficient. The overestimation, again, can be seen in both Figure 5.3 and Table 5.2. Within Figure 5.3, the global rotation method results fall slightly above the expected trendline. While in Table 5.2, all the percent differences associated with the global rotation method are positive. The positive percent differences indicate that the simulation is outputting a value above the expected result.

Additionally, the local rotation (sliding) method has a smaller percent difference when looking at all five trials. The local rotation (sliding) method has an average percent difference of -0.24%,

while the global rotation method has an average percent difference of 0.39%. All percent differences are below 3%, meaning all of the results are acceptable.

When increasing the level of the initial mesh size, the values for the heat transfer coefficient are to approach the results predicted by the Nusselt number correlation given in [9]. The results obtained when the level of the initial mesh size was increased to a value of 2 are shown in Figure 5.4 and Table 5.3.

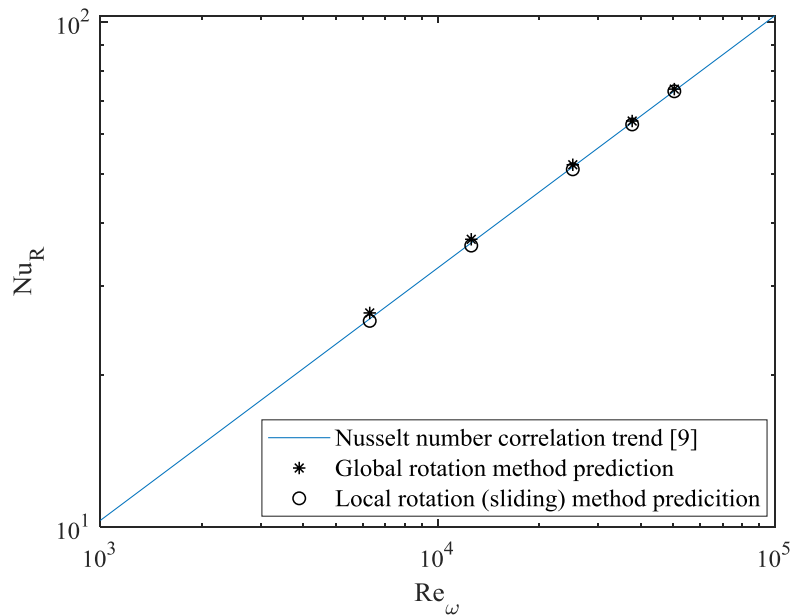


Figure 5.4: Results obtained for the both methods using a level of the initial mesh size of 2

Table 5.3: Summary of the results for both methods when the initial mesh level is set at 2

Angular velocity (rad/sec)	Rotational Reynolds number	Expected result from [9] (W/m <sup>2</sup> -K)	Global rotation results (W/m <sup>2</sup> -K)	Percent difference (%)	Local rotation results (W/m <sup>2</sup> -K)	Percent difference (%)
0.5	6.29E+03	1.5265	1.5682	0.67	1.5123	-0.23
1.0	1.26E+04	2.1588	2.1943	0.41	2.1320	-0.31
2.0	2.52E+04	3.0530	3.0830	0.24	3.0195	-0.28
3.0	3.78E+04	3.7391	3.7637	0.16	3.7055	-0.23
4.0	5.04E+04	4.3176	4.3536	0.21	4.3102	-0.04

Initial observations seen from the results obtained at a level of the initial mesh size of 2 are that both methods have a lower average percent difference when considering all five trials. The percent difference of the global rotation fell from an average value for all five trials of 0.39% to 0.34%. The average percent difference for the local rotation (sliding) method across the five trials fell from -0.24% to -0.22%. Showing that this mesh change is aiding both methods in approaching the expected results as outlined by the Nusselt number correlation given by [9].

However, for the local rotation (sliding) method, not all five trials saw a decrease in their respective percent difference. For example, with an angular velocity of 0.5 rad/sec, the percent difference increased in value from -0.07% to -0.23% when the mesh was changed from an initial mesh level of 1 to an initial mesh level of 2. The increase in percent difference shows that this method is more unpredictable when compared to the global rotation method.

The global rotation method, in contrast, saw the percent difference decrease in all five trials. Similar to what was observed when the level of the initial mesh size was a value of 1, the global rotation method overestimates the value of the heat transfer coefficient, while the local rotation (sliding) method underestimates the value. Figure 5.5 and Table 5.4 summarizes the results obtained after the level of the initial mesh size was increased to a value of 3.

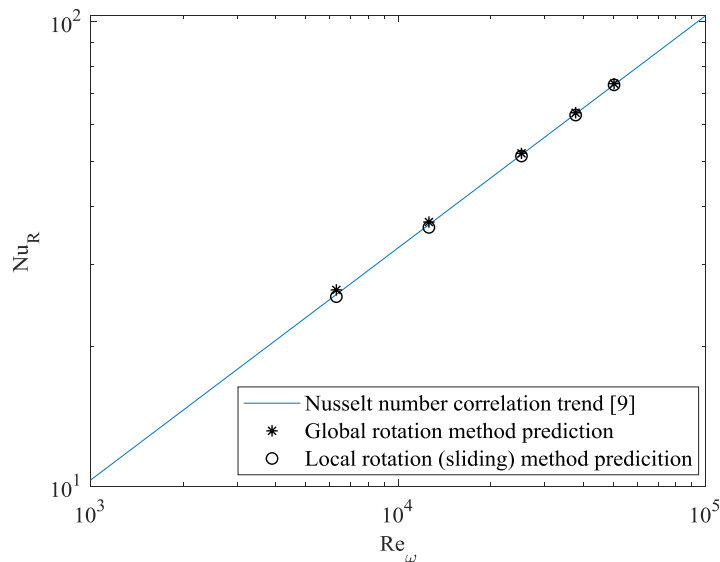


Figure 5.5: Results obtained for the both methods using a level of the initial mesh size of 3

Table 5.4: Summary of the results for both methods when the initial mesh level is set at 3

<b>Angular velocity (rad/sec)</b>	<b>Rotational Reynolds number</b>	<b>Expected result from [9] (W/m<sup>2</sup>-K)</b>	<b>Global rotation results (W/m<sup>2</sup>-K)</b>	<b>Percent difference (%)</b>	<b>Local rotation results (W/m<sup>2</sup>-K)</b>	<b>Percent difference (%)</b>
<b>0.5</b>	6.29E+03	1.5265	1.5617	0.57	1.5104	-0.27
<b>1.0</b>	1.26E+04	2.1588	2.1865	0.32	2.1291	-0.35
<b>2.0</b>	2.52E+04	3.0530	3.0738	0.17	3.0330	-0.16
<b>3.0</b>	3.78E+04	3.7391	3.7589	0.13	3.7159	-0.16
<b>4.0</b>	5.04E+04	4.3176	4.3428	0.15	4.3165	-0.01

When looking at the results obtained when the level of the initial mesh size was a value of 3, the trend of the global rotation overestimating the value of the heat transfer coefficient holds. While the local rotation (sliding) method continues to underestimate the value of the heat transfer coefficient, also, both methods saw a decrease in the average percent difference when considering all five trials. The global rotation fell from the previous average percent difference of 0.34% to 0.27%. The local rotation (sliding) method decreased in the average percent difference— falling from the previous percent difference of -0.22% to an average percent difference of -0.19%.

The local rotation (sliding) method requires a secondary body to simulate the rotation of the disk. In contrast, the global rotation method does not require a secondary body to simulate rotation. As a result, when discretizing the domain within the CFD simulation, additional cells are placed near the boundary of the secondary body when using the local rotation (sliding) method. The placement of the additional cells causes the difference between the two methods when estimating the convective heat transfer coefficient.

Both the global rotation method and local rotation (sliding) method continued to approach a value similar to the one predicted by the Nusselt number correlation given by [9]. The level of the initial mesh size is again increased from a value of 3 to a value of 4. The results are summarized in Figure 5.6 and Table 5.5 for the level of the initial mesh size of 4.

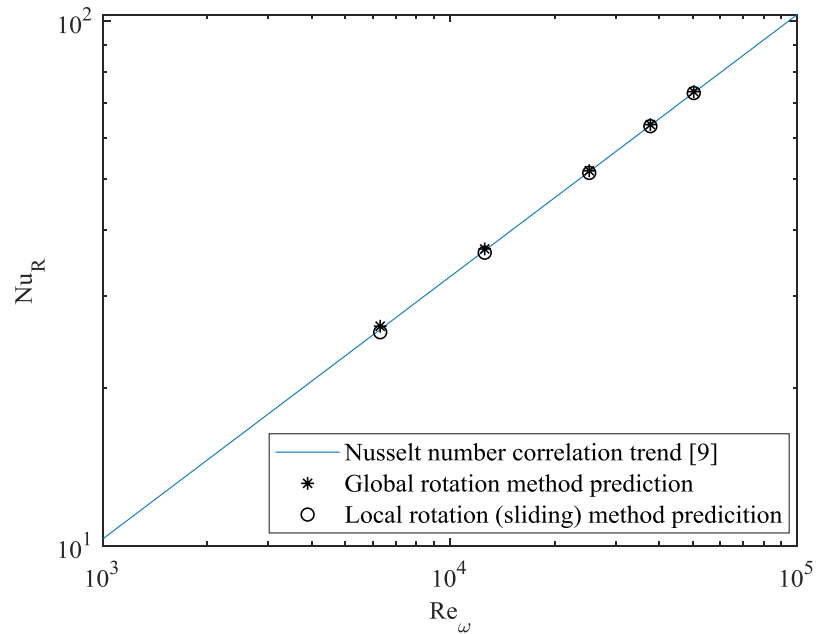


Figure 5.6: Results obtained for the both methods using a level of the initial mesh size of 4

Table 5.5: Summary of the results for both methods when the initial mesh level is set at 4

Angular velocity (rad/sec)	Rotational Reynolds number	Expected result from [9] (W/m <sup>2</sup> -K)	Global rotation results (W/m <sup>2</sup> -K)	Percent difference (%)	Local rotation results (W/m <sup>2</sup> -K)	Percent difference (%)
<b>0.5</b>	6.29E+03	1.5265	1.5483	0.35	1.5080	-0.31
<b>1.0</b>	1.26E+04	2.1588	2.1738	0.17	2.1384	-0.24
<b>2.0</b>	2.52E+04	3.0530	3.0646	0.10	3.0357	-0.14
<b>3.0</b>	3.78E+04	3.7391	3.7533	0.09	3.7271	-0.08
<b>4.0</b>	5.04E+04	4.3176	4.3370	0.11	4.3113	-0.04

When increasing the level of the initial mesh size to a value of 4, the global rotation method saw a decrease in average percent difference — falling from a value of 0.27% to a value of 0.17% seen in Table 5.5. Similarly, the local rotation (sliding) method saw a decrease in the value of the average percent difference. The value was at -0.19% and decreased to a value of -0.16%. Additionally, the local rotation (sliding) method saw an increase in percent difference when

increasing the level of the initial mesh size from 3 to 4 for angular velocities of 0.5 rad/sec and 4.0 rad/sec, showing the unpredictability when using the method.

The global rotation method continues to approach the expected values. By approaching the predicted values without underestimating, the global rotation method shows it is better suited for individual bodies being analyzed, while the local rotation (sliding) method is best employed when many different sources cause the heat transfer. For example, a small piece in a computer may be rotating and have a stationary heat source next to it. For this example, the local rotating region (sliding) method should be used.

The global rotation method is recommended when capturing the results for a single body. Reasons for using the global rotation method over the local rotating region (sliding) method are listed below:

- The global rotational method did not underestimate the results for the heat transfer coefficient when compared to the results obtained from the Nusselt number correlations.
- The global rotation method simulates rotation without the need for introducing a secondary body.
- The introduction of a secondary body to simulate rotation in the local rotation (sliding) method introduces inaccuracies around the secondary body when creating the mesh throughout the domain.
- The global rotation region method showed the values of all trials approaching the expected values as the level of the initial mesh size increased.
- The global rotating method does not need to have an investigation into the size of the secondary body. When using the local rotation (sliding) method, the secondary body does impact the results when the second body is too small.

Before continuing with the turbulent regime, it is necessary to test out higher angular velocities within the laminar regime. Similar to the procedure followed before, the mesh settings are kept the same for each trial. Table 5.6 shows the input variables for the parametric study. Table 5.7 shows the boundaries for all the flow regimes. Figure 5.7 and Table 5.8 summarize the results obtained when the level of the initial mesh was set to 5, and higher angular velocities are tested.

Table 5.6: Parametric study input variables

<b>Level of the initial mesh</b>	1, 2, 3, 4, 5
<b>Angular velocity (rad/sec)</b>	0.5, 1.0, 2.0, 3.0, 4.0, 5.0, 6.0, 7.0

Table 5.7: Flow regime boundaries

<b>Flow Regime</b>	<b>Reynolds Number Value</b>
<b>Laminar</b>	$Re_\omega < 10^5$
<b>Transition</b>	$10^5 \leq Re_\omega < 10^6$
<b>Turbulent</b>	$Re_\omega \geq 10^6$

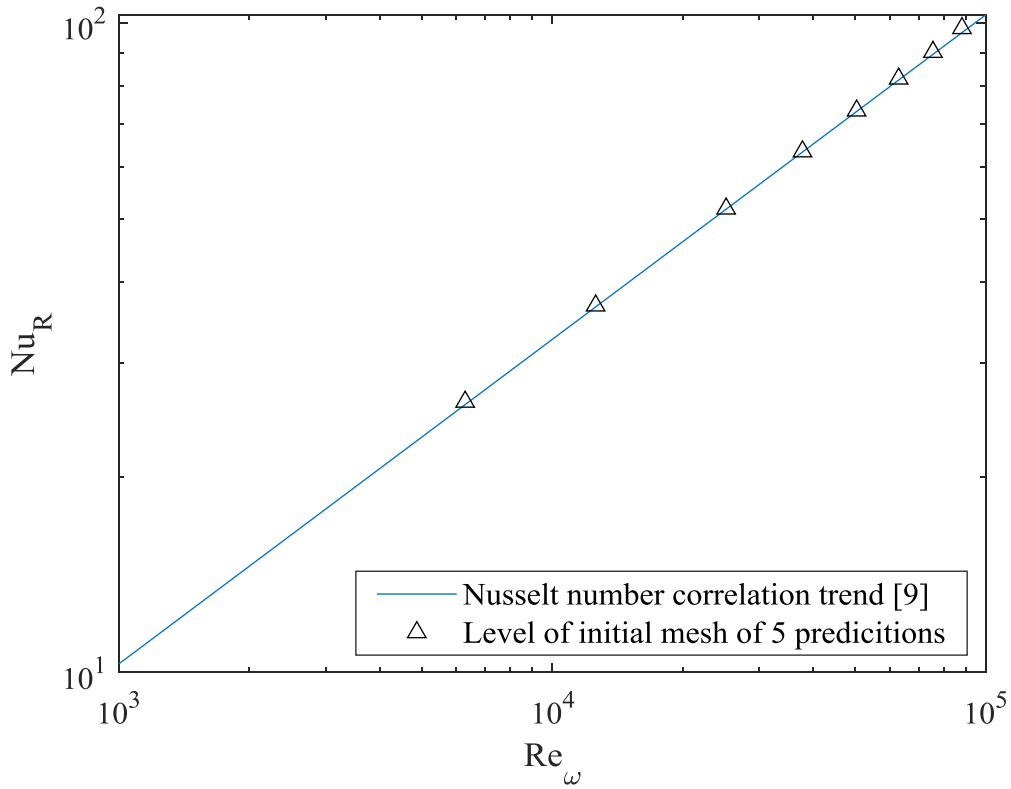


Figure 5.7: Higher angular velocities tested with a level of the initial mesh size of 5

Table 5.8: Global rotation results at higher angular velocities and level of initial mesh of 5

<b>Angular velocity (rad/sec)</b>	<b>Rotational Reynolds number</b>	<b>Expected heat transfer coefficient value (W/m<sup>2</sup>-K)</b>	<b>Results mesh size:5 (W/m<sup>2</sup>-K)</b>	<b>Percent difference (%)</b>
<b>0.5</b>	6.29E+03	1.5265	1.5416	0.25
<b>1.0</b>	1.26E+04	2.1588	2.1687	0.11
<b>2.0</b>	2.52E+04	3.0530	3.0586	0.05
<b>3.0</b>	3.78E+04	3.7391	3.7465	0.05
<b>4.0</b>	5.04E+04	4.3176	4.3308	0.08
<b>5.0</b>	6.29E+04	4.8272	4.8503	0.12
<b>6.0</b>	7.55E+04	5.2879	5.3319	0.21
<b>7.0</b>	8.81E+04	5.7116	5.8011	0.39

An initial observation from Figure 5.7 and Table 5.8 is that the global rotation method continues to overestimate the heat transfer coefficient even at higher angular velocities within the laminar regime. Also, the results continue to converge towards the expected values. When the level of the initial mesh size was 4, the average percent difference for these five trials was 0.17%, and as the level of the initial mesh size was increased to a value of 5, the average percent difference dropped to 0.11%. The average percent difference for all angular velocities tested at a level of the initial mesh of 5 was 0.16%.

Table 5.9 and Table 5.10 show the results for all global rotation simulations and the percent difference for each result. Table 5.9 and Table 5.10 shows the angular velocities tested, the level of the initial mesh size, the rotational Reynolds number, the expected result when using the relation from [9], the results obtained from the CFD simulation, and the percent difference between the results from the CFD simulation and the relation from [9]. Both tables aid in showing the convergence of the global rotation method as the level of the initial mesh varied.

Table 5.9: Summary of global rotation method results near the beginning of the laminar regime

Angular velocity (rad/s)	0.5		1.0		2.0		3.0	
Rotational Reynolds number	6.29E+03		1.26E+04		2.52E+04		3.78E+04	
Level of initial mesh size	Simulation results (W/m <sup>2</sup> .K)	Percent difference (%)	Simulation results (W/m <sup>2</sup> .K)	Percent difference (%)	Simulation results (W/m <sup>2</sup> .K)	Percent difference (%)	Simulation results (W/m <sup>2</sup> .K)	Percent difference (%)
1	1.5709	0.72	2.1966	0.43	3.0875	0.28	3.7639	0.16
2	1.5682	0.67	2.1943	0.41	3.0830	0.24	3.7637	0.16
3	1.5617	0.57	2.1865	0.32	3.0738	0.17	3.7589	0.13
4	1.5483	0.35	2.1738	0.17	3.0646	0.10	3.7533	0.09
5	1.5416	0.25	2.1687	0.11	3.0586	0.05	3.7465	0.05
Results from [9]	1.5265		2.1588		3.0530		3.7391	

Table 5.10: Summary of global rotation method results near the end of the laminar regime

Angular velocity (rad/s)	4.0		5.0		6.0		7.0	
Rotational Reynolds number	5.04E+04		6.29E+04		7.55E+04		8.81E+04	
Level of initial mesh size	Simulation results (W/m <sup>2</sup> .K)	Percent difference (%)	Simulation results (W/m <sup>2</sup> .K)	Percent difference (%)	Simulation results (W/m <sup>2</sup> .K)	Percent difference (%)	Simulation results (W/m <sup>2</sup> .K)	Percent difference (%)
1	4.3770	0.34	4.9616	0.69	5.4589	0.80	5.8966	0.80
2	4.3536	0.21	4.9162	0.46	5.4419	0.72	5.8975	0.80
3	4.3428	0.15	4.8846	0.30	5.4128	0.58	5.8924	0.78
4	4.3370	0.11	4.8660	0.20	5.3780	0.42	5.8672	0.67
5	4.3308	0.08	4.8503	0.12	5.3319	0.21	5.8011	0.39
Results from [9]	4.3176		4.8272		5.2879		5.7116	

Having verified the physics of the CFD simulation in Chapter 3, and validated the results in Chapter 5, the next step is to test the boundaries of the simulation, which can be done by examining all flow regimes: laminar, transition, and turbulent. However, before conducting a turbulent test, the turbulence parameters must be determined. The turbulence parameters can be found by determining values that allow for coarse meshes to estimate the heat transfer coefficient accurately.

## 6. TESTING FOR FULL RANGE OF ROTATIONAL SPEEDS

### 6.1 Description of Rotational Regimes for Different Reynolds Number

When considering the flow of a fluid due to rotation, the flow regimes are described as laminar, transition, and turbulent based on the rotation Reynolds number. Table 6.1 summarizes the values for which each regime is applicable.

Table 6.1: Rotational Reynolds number for each flow regime for a rotating disk in still air

Flow Regime	Reynolds Number Value
Laminar	$Re_{\omega} < 10^5$
Transition	$10^5 \leq Re_{\omega} < 10^6$
Turbulent	$Re_{\omega} \geq 10^6$

Within this chapter, the heat transfer coefficient is found for transition and turbulent regimes for a rotating disk in still air by utilizing the global rotation method. SolidWorks provides the user with the ability to define the flow regime that is being studied when initializing the CFD software. Figure 6.1 shows this step.

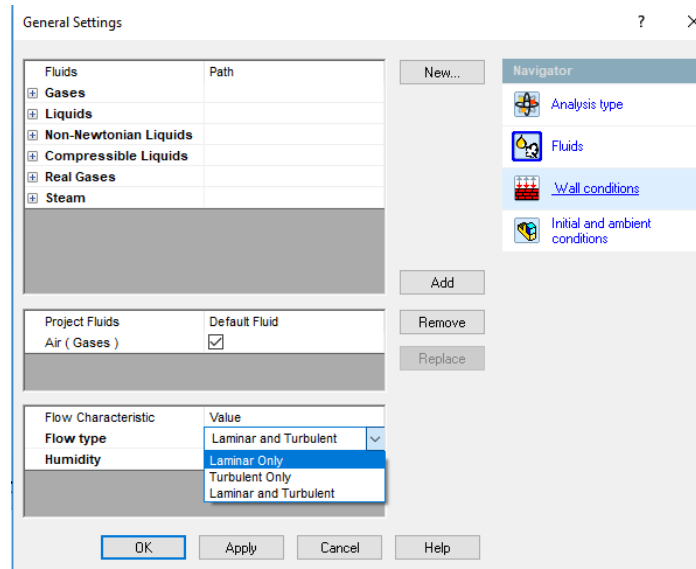
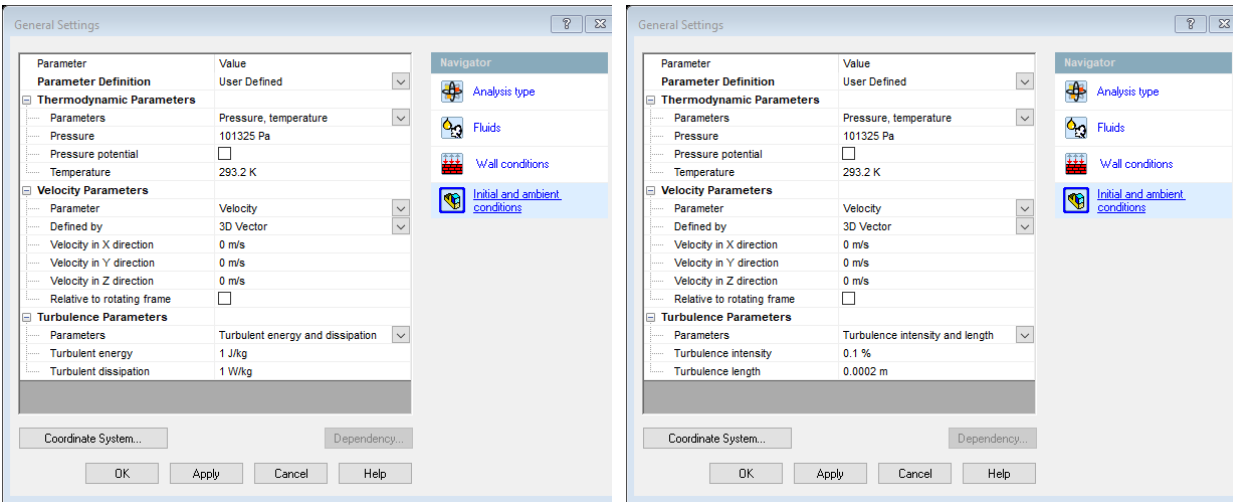


Figure 6.1: Available options for the flow type when initializing the CFD simulation

When using the option ‘*Laminar Only*,’ the turbulent parameters are not present, and the CFD software solves the simulation assuming all flow in the domain is laminar. Utilizing the option ‘*Turbulent Only*’ causes the CFD software to proceed under the assumption that the flow throughout the entire domain is turbulent. By using the ‘*Turbulent Only*’ setting, the user must also define the turbulence parameters. The available options for defining the turbulence parameters are either by the turbulent energy and dissipation rate, or turbulence intensity and length. Figure 6.2 shows the default settings for definitions of the turbulent parameters within SolidWorks.



(a)

(b)

Figure 6.2: Default settings for the two definitions of the turbulence parameters

The third option that can be utilized is ‘*Laminar and Turbulent*.’ This option does not make assumptions about the flow; however, the user must still define the turbulence parameters. The same default settings for the turbulence parameters appear when using the option ‘*Laminar and Turbulent*.’

The generation of the CFD simulation for a turbulent regime is similar to the methods used when generating a CFD simulation when analyzing a laminar flow. The one difference between the procedure for a turbulent regime is the user defining the turbulence parameters. From the SolidWorks technical reference [11], the recommended setting is the ‘*Turbulence energy and dissipation*’ option as opposed to the ‘*Turbulence intensity and length*.’ The following section outlines the procedure for generating the simulation.

### 6.1.1 Detailed Procedure for Various Rotational Speeds

1. For this, a disk similar to the one outlined in Chapter 3 was generated. The disk is 1 meter in diameter and 20 millimeters in thickness.
2. The CFD software is initialized and named accordingly.
3. Select the units used within the CFD simulation.
4. Define the analysis type and physical features.
5. Select the working fluid.
6. Apply the correct temperature onto the disk.
7. Define the settings for the first flow regime. Figure 6.3 shows the turbulent parameters. The values for the turbulence parameters were found by using a parametric study that allowed SolidWorks to test for various values. The parametric study concluded that the values shown in Figure 6.3 accurately predicted the heat transfer coefficient values without underestimating the heat transfer coefficient when using fine meshes.

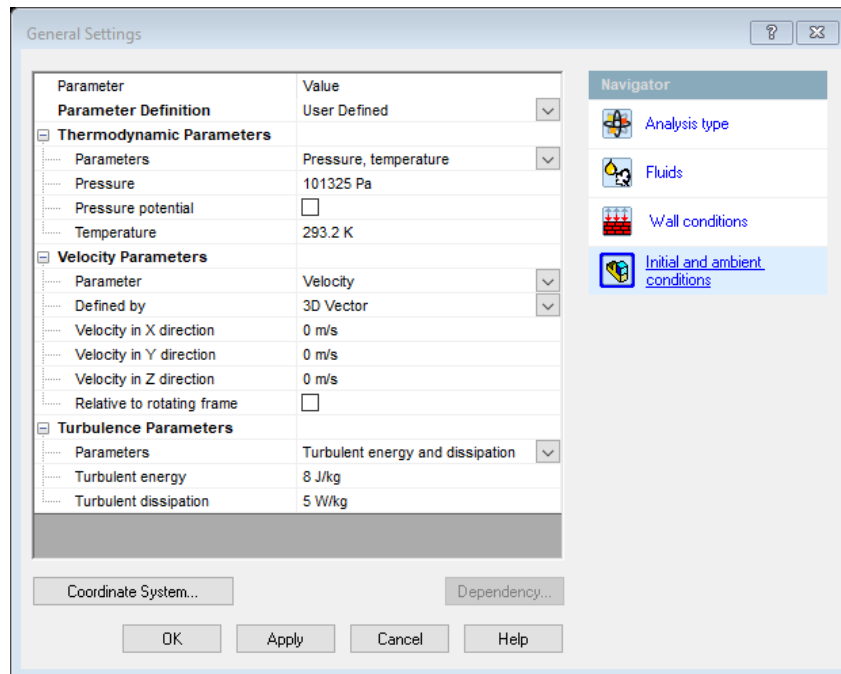


Figure 6.3: Turbulence parameters used for the turbulent simulation

8. Set the domain size to be a cube of 3 meters in length.
9. Set an adiabatic boundary condition on the side and bottom surface of the disk.

10. Generate a global mesh. A local mesh is made similar to the local mesh made in Chapter 4. The setting used to differentiate the mesh size is the level of the initial mesh size for an automatic mesh shown in Figure 6.4.

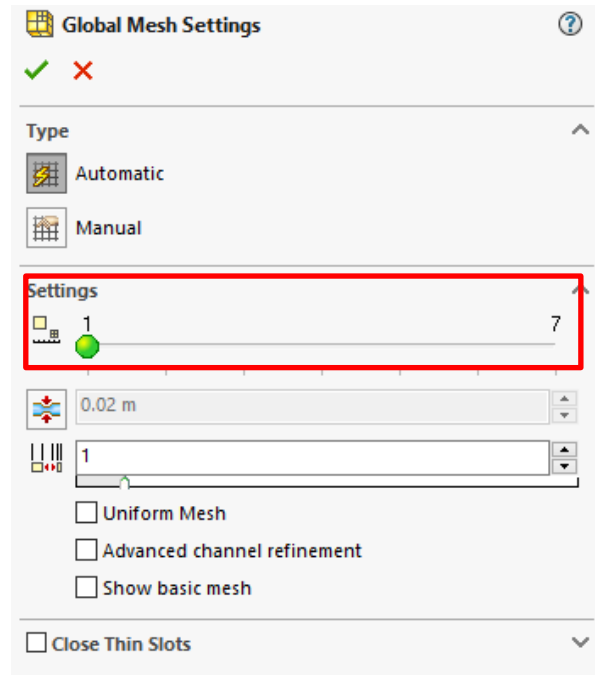


Figure 6.4: Setting used to change the mesh size for each simulation conducted

11. The convergence parameter is set to 3%. The convergence parameter is used as the maximum acceptable percent difference. Predications with a percent difference above 3% are deemed unacceptable, and predications with percent differences below 3% are deemed acceptable.
12. Start the simulation.

## 6.2 Validation of Various Rotational Rates

When attempting to simulate the turbulent regime, the settings that were changed included the flow regime. For the turbulent simulations, the flow regime was defined as *'Turbulent Only'* within the simulation settings. The turbulent parameters used are turbulent energy and turbulent dissipation and were set to a value of 8 and 5, respectively. The results from the simulation are

compared to the expected results predicted by the Nusselt number correlation, given by Dorfman [2],

$$Nu_R = \frac{\bar{h}R}{k} = 0.01486 * Re_{\omega}^{0.8}. \quad 6.1$$

A parametric study was conducted to obtain results for various trials. Before starting the parametric study, the user must define both the input variables that can be monitored and changed if desired and define the output parameters. For all simulations, the input variables were the angular velocity, the turbulence parameters, and the level of the initial mesh. Table 6.2 shows the values used in these settings. The only output parameter that was defined is the heat transfer coefficient.

Table 6.2: Parametric study input variables for turbulent simulations

<b>Level of the initial mesh</b>	1, 2, 3, 4, 5, 6, 7
<b>Angular velocity (rad/sec)</b>	90, 95, 100, 105, 110, 115, 120, 125
<b>Turbulent Energy (J/kg)</b>	8
<b>Turbulent Dissipation (W/kg)</b>	5

Figure 6.5 summarizes the results for all mesh sizes tested while the tables compare the results between two mesh sizes. Table 6.3 and Table 6.4 summarize the results for all simulations. Included in each table are the angular velocity being tested, the resulting rotational Reynolds number, the level of the initial mesh size, the resulting heat transfer coefficient, the expected result from [2], and the percent difference between the result from the CFD simulation and the result predicted by [2]. Table 6.3, and Table 6.4 show how the simulation results converge to the expected values as the level of the initial mesh size increased. The first and second row of Table 6.3. and Table 6.4 shows the results obtained for a level of the initial mesh of 1 and 2.

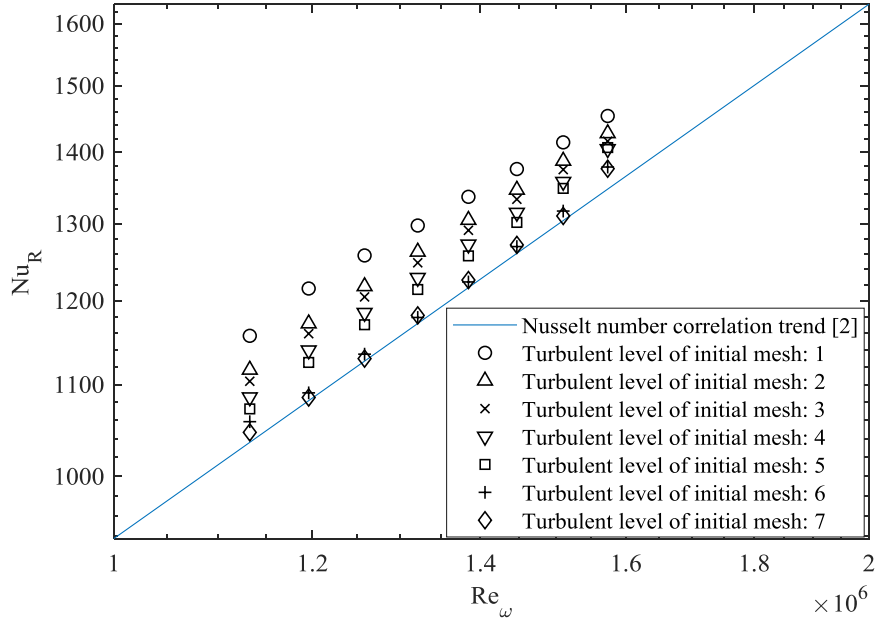


Figure 6.5: Turbulent results obtained for initial mesh level of 1 and 2

Table 6.3: Summary of global rotation method results at low, turbulent Reynolds number

Angular velocity (rad/s)	90		95		100		105	
Rotational Reynolds number	1.13E+06		1.20E+06		1.26E+06		1.32E+06	
Level of initial mesh size	Simulation results (W/(m <sup>2</sup> .K))	Percent difference (%)	Simulation results (W/(m <sup>2</sup> .K))	Percent difference (%)	Simulation results (W/(m <sup>2</sup> .K))	Percent difference (%)	Simulation results (W/(m <sup>2</sup> .K))	Percent difference (%)
1	68.3190	2.76	71.7559	2.91	74.2603	2.74	76.6035	2.54
2	65.9497	1.88	69.1930	2.00	71.9187	1.94	74.5412	1.86
3	65.1727	1.58	68.4702	1.74	71.1337	1.67	73.6987	1.58
4	64.1023	1.17	67.3016	1.31	69.9744	1.25	72.5627	1.19
5	63.3294	0.87	66.4577	0.99	69.1094	0.94	71.6846	0.88
6	62.4957	0.54	64.3931	0.20	67.0311	0.18	69.6327	0.16
7	61.8062	0.26	64.0822	0.08	66.7212	0.07	69.7824	0.21
Results from [2]	61.1685		63.8723		66.5478		69.1967	

Table 6.4: Summary of global rotation method results at higher, turbulent Reynolds number

Angular velocity (rad/s)	110		115		120		125	
Rotational Reynolds number	1.38E+06		1.45E+06		1.51E+06		1.57E+06	
Level of initial mesh size	Simulation results (W/(m <sup>2</sup> .K))	Percent difference (%)	Simulation results (W/(m <sup>2</sup> .K))	Percent difference (%)	Simulation results (W/(m <sup>2</sup> .K))	Percent difference (%)	Simulation results (W/(m <sup>2</sup> .K))	Percent difference (%)
1	78.9202	2.35	81.2285	2.19	83.5074	2.03	85.8260	1.90
2	77.0413	1.75	79.4909	1.65	81.9153	1.55	84.2904	1.45
3	76.2250	1.49	78.7192	1.40	81.1794	1.32	83.6087	1.24
4	75.1180	1.12	77.6334	1.06	80.1628	1.01	82.9358	1.04
5	74.2281	0.82	76.8498	0.80	79.6136	0.84	83.0587	1.08
6	72.2464	0.15	74.9487	0.18	77.7620	0.25	81.3969	0.57
7	72.3894	0.20	75.0782	0.22	77.3671	0.12	81.2554	0.53
Results from [2]	71.8204		74.4204		76.9979		79.5540	

An initial observation that can be made from Figure 6.5, Table 6.3, and Table 6.4 is that the value for the heat transfer coefficient is predicted well when using an initial mesh level of 1 and 2. All trials resulted in a percent difference below 3%. Additionally, the average percent difference is decreasing as the level of the initial mesh is increasing. The average percent difference fell from a value of 2.43% to 1.76% as the level of the initial mesh size is increased.

When increasing the level of the initial mesh size, the spacing between each cell is smaller, discretizing the domain into a finer mesh. Due to this, the value of the heat transfer coefficient obtained from the CFD simulation is expected to get closer predicted values from the Nusselt number correlation. Figure 6.5 shows that this does indeed occur when the level of mesh size is increased. The third and fourth row of Table 6.3 and Table 6.4 summarize the results obtained when the level of the initial mesh size was a value of 3 and 4 respectively.

By increasing the level of the initial mesh size to values of 3 and 4, the heat transfer is converging towards the expected values. An observation from Table 6.3 and Table 6.4 is that all trials resulted in a percent difference below 3%. Additionally, the heat transfer continues to converge towards the expected values as predicted by the correlation given by [2]. The convergence is seen in Figure 6.5 and from the average percent differences. For a level of the initial mesh of 3, the percent difference was 1.50%, while the average percent difference for the level of the initial mesh of 4

was 1.14%. The fifth and sixth row of Table 6.3 and Table 6.4 summarize the results obtained when the level of the initial mesh size was a value of 5 and 6 respectively.

When the level of the initial mesh size is set to a value of 5, all the percent differences are below 3% — indicating that the values obtained for the heat transfer coefficient are acceptable. Once the level of the initial mesh size is set to 6, all trials also achieved a percent difference below 3%. The convergence towards the expected values predicted by the correlation given by [2] is seen in Figure 6.5, and the average percent differences continue to decrease as the level of the initial mesh is increased. The average percent difference for an initial mesh level of 5 is 0.90%, and the average percent difference for a level of the initial mesh size of 6 is 0.28%. The level of the initial mesh size is increased to 7 to continue to see the convergence of the results with the predicted values obtained from the correlation given by Dorfman [2]. The seventh row of Table 6.3 and Table 6.4 summarize the results obtained when the level of the initial mesh size was a value of 7.

By having the level of the initial mesh size set to a value of 7, all the percent differences are below 3% — indicating that the values obtained for the heat transfer coefficient are acceptable. The convergence towards the expected values predicted by the correlation given by [2] is seen in Figure 6.5, and the average percent differences continue to decrease as the level of the initial mesh is increased. The average percent difference for an initial mesh level of 7 is 0.21%. The results for the turbulent regime are validated by having the percent differences below 3% and showcasing the convergence of the simulation predictions to the analytical correlation given by [2]. Figure 6.6 shows results for both laminar and turbulent regime as well as the level of the initial mesh.

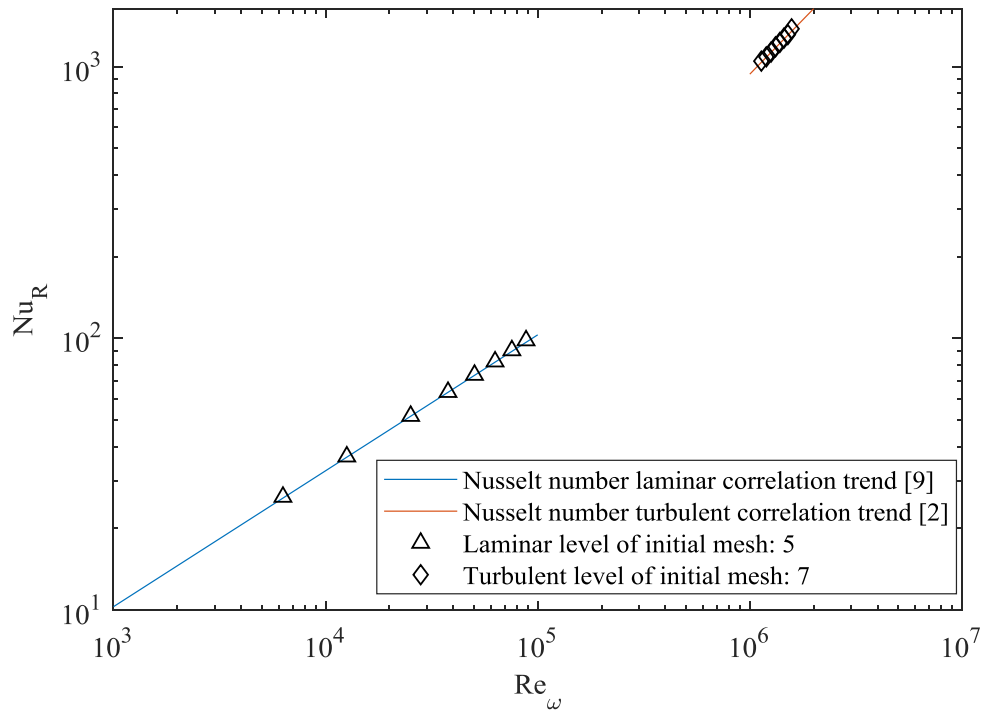


Figure 6.6: Summary of results for both laminar and turbulent regime

Both the laminar and turbulent simulation resulted in low average percent differences. For the laminar results, the average percent difference when the level of the initial mesh size was a value of 5 was 0.16%. For the turbulent results, the average percent difference when the level of the initial mesh size was a value of 7 was 0.21%. These low percent differences show that the SolidWorks CFD simulation is useful when simulating a rotating body and attempting to obtain accurate heat transfer coefficient values. However, an improvement for this study is the definition of the turbulence parameters. SolidWorks allows the user to create a dependency on these parameters. The dependency can read from a table, or an equation can relate the parameters to any of the variables available within the CFD simulation. The need for the turbulence parameters relation is further seen when attempting to capture the transition zone. Figure 6.7 shows the settings used for the transition zone simulations. The difference between the transition zone settings and the previous settings utilized is that the flow type is described as '*Laminar and Turbulent.*' The turbulent parameters were not changed from the default settings. In Figure 6.8, a box is around the dependency setting, and the turbulence parameters are shown, while Figure 6.9 shows the different user dependencies that can be defined for the turbulent parameters.

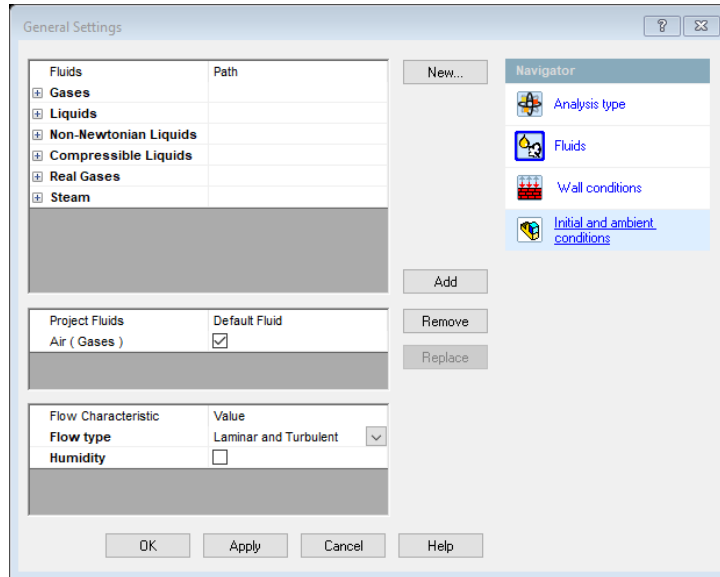


Figure 6.7: Flow type settings for the transition zone simulations

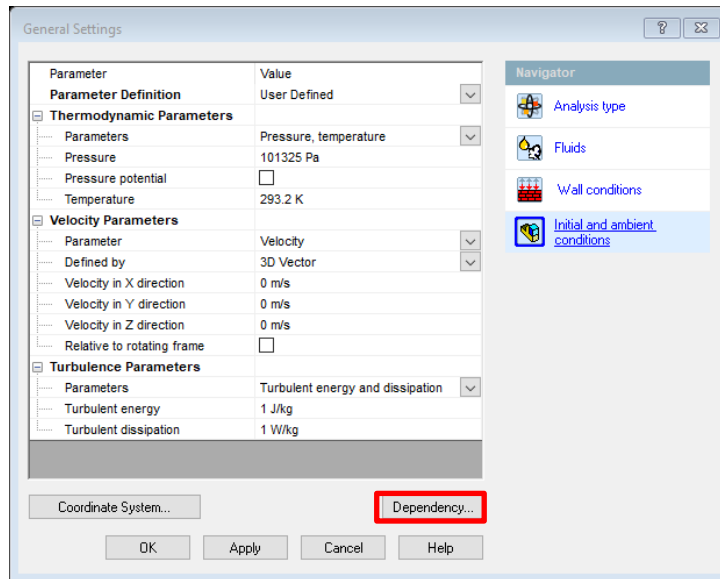


Figure 6.8: Turbulent parameters settings when simulating the transition zone

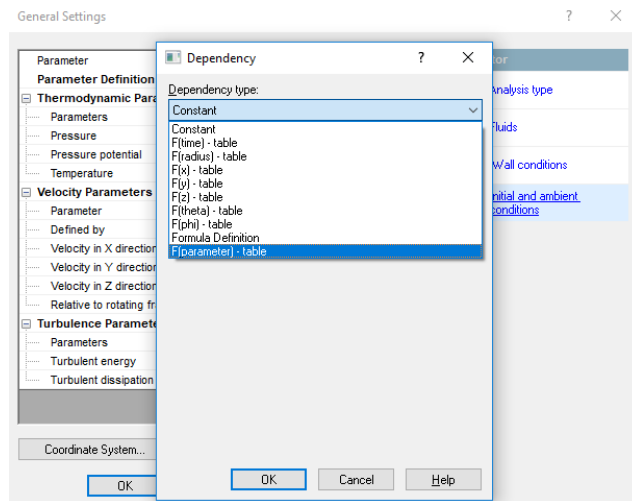


Figure 6.9: The dependency types available in SolidWorks CFD

For this study, the dependency setting was not used. Instead, the turbulent parameters were not changed from their default settings when testing within the transition regime. Figure 6.10 summarizes the results obtained for the transition zone.

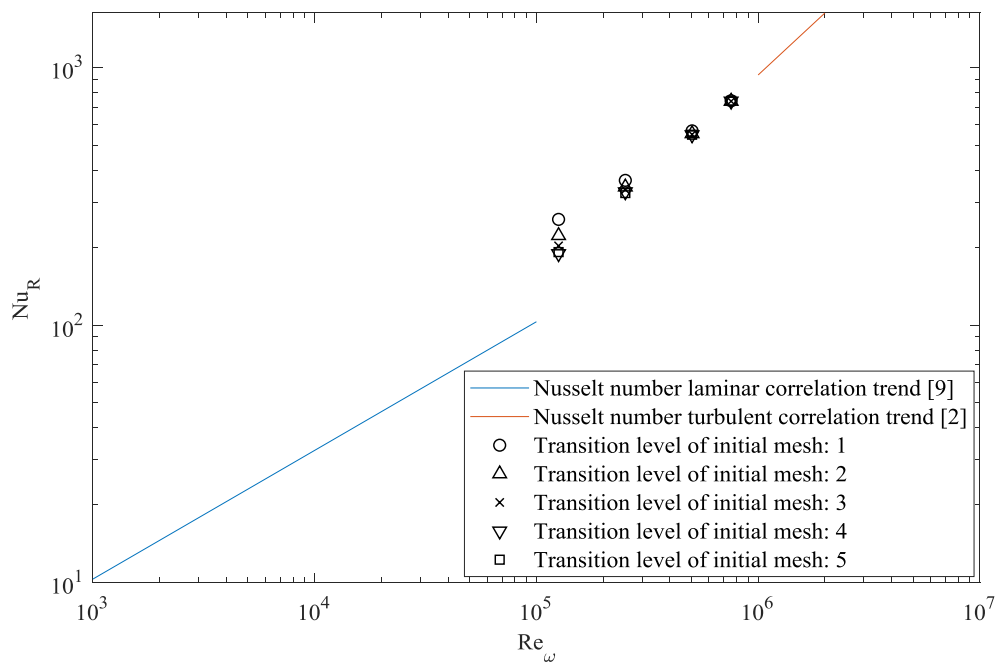


Figure 6.10: Simulation showing convergence in transition zone

Figure 6.10 further emphasizes the need to utilize a relation to define the turbulent parameters. By only using set values, a much finer mesh is needed at the lower end of the transition zone to obtain adequate precision. By having a relation that reads the fluid velocity, these inaccuracies can be avoided. Figure 6.11 summarizes the final results for all three regimes.

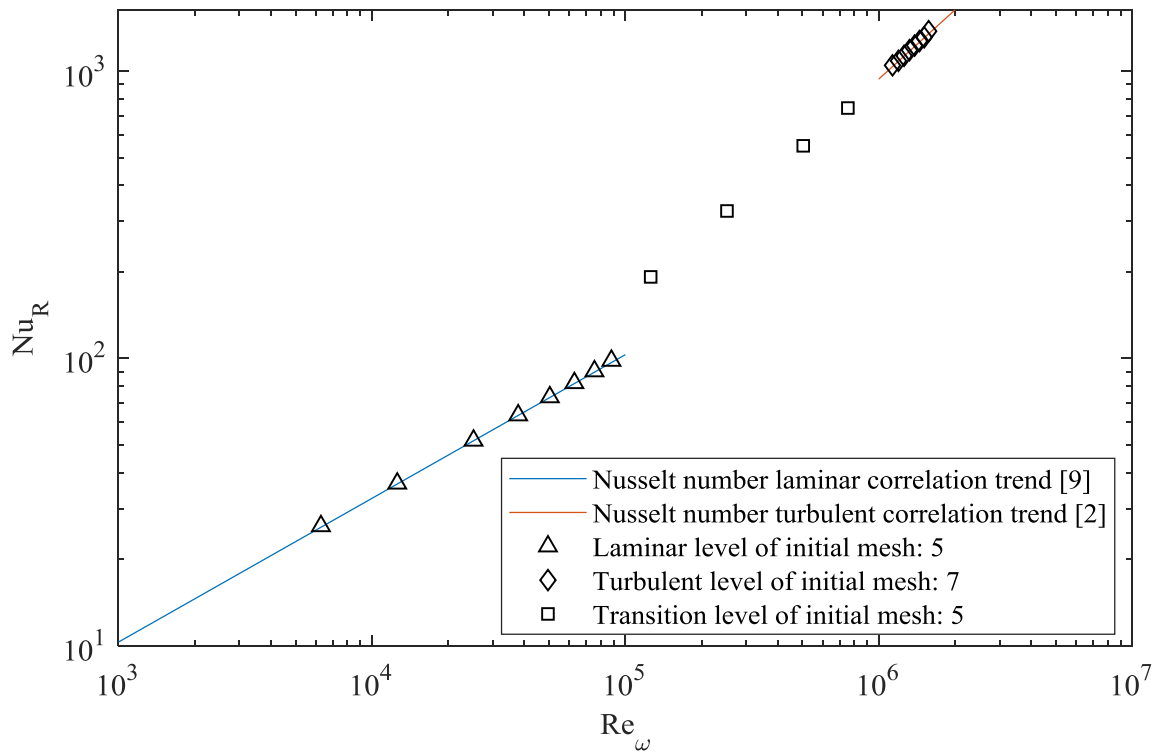


Figure 6.11: Results for all regimes

The CFD model was verified, and the CFD simulation was validated. The verification was done by obtaining the temperature and velocity profiles. The velocity profile for a spinning disk within the simulation must be independent of the coordinates of the radial position. The independence of the velocity profile was seen in Chapter 3. Additionally, Chapter 3 showed general trends that resulted when plotting the velocity and temperature profiles while varying the rotational rate and the radial position.

The validation of the CFD simulation is found in Chapter 5 and Chapter 6. Chapter 5 showed the results obtained for the heat transfer coefficient when using two different rotational simulation

methods. Both methods agreed with predicted results when using analytical correlations from previous works of literature. Chapter 6 showed the results for turbulent and transition regimes. The turbulent regime results agreed with the correlations found in works of literature.

## 7. IMPACT OF TOTAL AMOUNT OF CELLS ON SIMULATION TIME AND EXPECTED PERCENT DIFFERENCE

Additional items needed to characterize include the relation between the total amount of cells in a simulation and the time needed to complete the simulation, and the relation between the total amount of cells and the expected percent difference. This is done for both the laminar and turbulent regime.

Figure 7.1 shows how the simulation time varies with the total number of cells during the laminar regime simulations. Figure 7.2 shows how the percent difference is impacted by the total number of cells during the laminar regime simulations. Table 7.1 shows the total number of cells for each mesh level used during the laminar regime simulations. Additionally, the table shows the total number of cells contacting the solid disk, the cell ratio between the total cells and contacting cells, the time to complete the simulation, the amount of time to generate the mesh, the iterations predicted, the total amount of iterations to complete the simulation, and the average expected percent difference based on results from Table 5.9 and Table 5.10 found in Chapter 5.

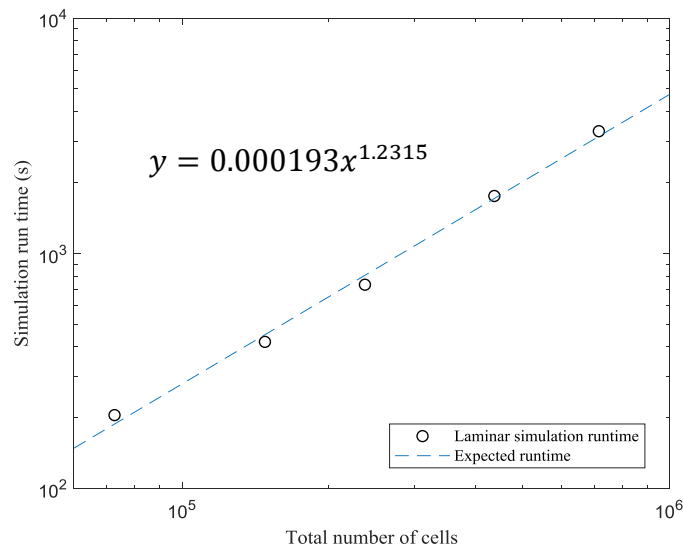


Figure 7.1: Laminar relation of the total number of cells and the simulation time

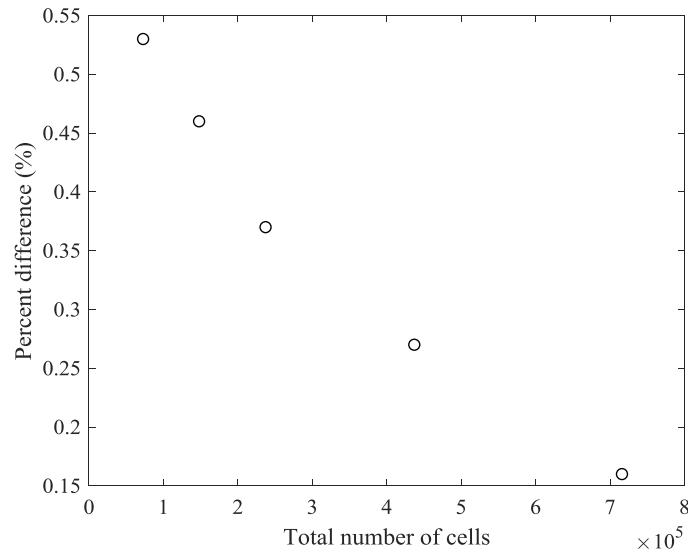


Figure 7.2: Laminar relation of the total number of cells and the expected percent difference

Table 7.1: Expected times and percent differences for the meshes tested in the laminar regime

Mesh level	Total cells	Contacting cells	Cell ratio	Simulation time (s)	Mesh time (s)	Iterations predicted	Total iterations	Expected percent difference (%)
<b>1</b>	72696	15288	21.03%	205	5	217	217	0.53
<b>2</b>	147912	27984	18.92%	420	7	275	275	0.46
<b>3</b>	237212	44072	18.58%	735	10	321	321	0.37
<b>4</b>	437008	86000	19.68%	1752	18	395	395	0.27
<b>5</b>	716014	141574	19.77%	3304	28	465	465	0.16

Based on Figure 7.1, Figure 7.2, and Table 7.1, an increase in the number of cells decreases the percent difference, but one must also consider the amount of time the simulation takes to complete. Depending on the accuracy needed within the laminar regime, one may need a fine mesh, above 700000 cells, or a coarse mesh, below 100000 cells. If a percent difference below 0.6% is needed, then a mesh consisting of 72000 cells is sufficient. This mesh will complete the simulation in around 250 seconds. Now if a percent difference below 0.2% is needed then the mesh must have at least 600000 cells meaning the simulation will be completed after 2500 seconds.

While conducting the turbulent regime simulations, an observation is that the simulation times are longer than the times found for the laminar regime. This is due to the number of iterations needed to complete the simulation. During the laminar regime simulations, the iterations predicted to complete the simulation match the total number of iterations, while during the turbulent regime

the number of predicted iterations is lower than the number of iterations taken to complete the simulations. Table 7.2 shows this occurring for all meshes used in the turbulent regime. When comparing Table 7.1 and Table 7.2 an observation seen is that the expected percent difference for a specific mesh is higher during the turbulent regime simulation than during the laminar regime. Meaning that a much finer mesh must be used to achieve the percent differences seen during the laminar regime simulations. The percent difference during the turbulent regime simulations did not reach the levels of the laminar regime percent differences until a mesh size consisting of 1381152 cells. This corresponded to a time of 10914 seconds. During the laminar regime the first mesh used only consisted of 72696 cells and achieved a percent difference of 0.53% in 205 seconds.

Table 7.2: Expected times and percent differences for the meshes tested in the turbulent regime

Mesh level	Total cells	Contacting cells	Cell ratio	Simulation time (s)	Mesh time (s)	Iterations predicted	Total iterations	Expected percent difference (%)
1	72696	15288	21.03%	274	4	217	274	2.43
2	147912	27984	18.92%	649	6	275	339	1.76
3	237212	44072	18.58%	1111	8	321	393	1.50
4	437008	86000	19.68%	2507	17	395	488	1.14
5	716014	141574	19.77%	4605	27	465	572	0.90
6	1381152	292762	21.20%	10914	57	581	708	0.28
7	2421594	557164	23.01%	23169	105	701	841	0.21

When comparing the relations obtained for the laminar and turbulent regimes, the simulation time behaves similarly for both regimes. Both regimes have the simulation time being proportional to the total number of cells raised to a power and multiplied by a constant. This is seen in Figure 7.1 and Figure 7.3.

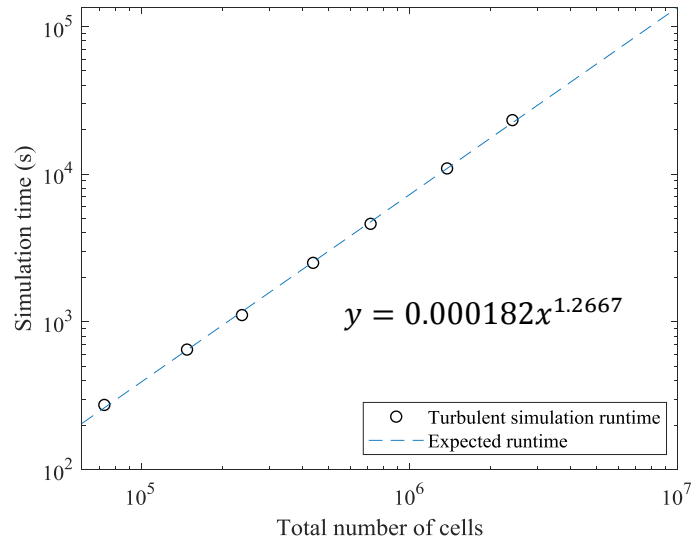


Figure 7.3: Turbulent relation of the total number of cells and the simulation time

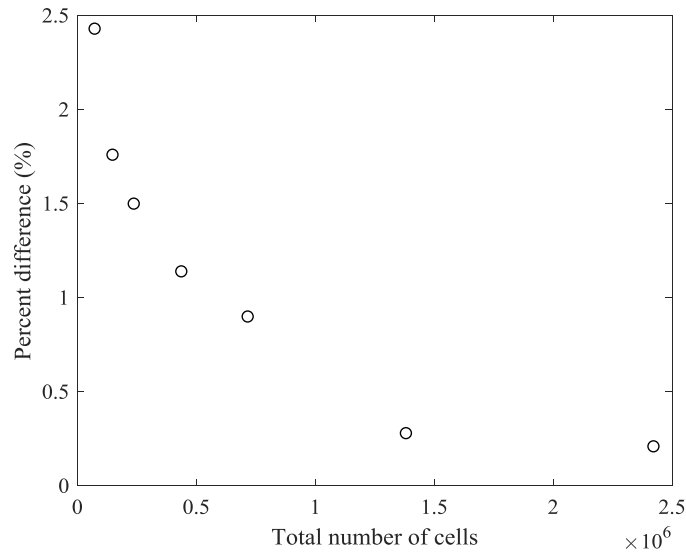


Figure 7.4: Turbulent relation of the total number of cells and the expected percent difference

Based on the information in Figure 7.3, Figure 7.4, and Table 7.2, the turbulent regime requires a fine mesh to achieve a percent difference below 1%, while in contrast, the laminar regime can obtain a percent difference below 1% with a coarse mesh. If a percent difference below 1% is desired, then the minimum number of cells needed is 500000, which corresponds to a time of 5000 seconds.

## 8. CONCLUSION

Having obtained results that agree with the reported correlations from previous literature for both the laminar and turbulent regime, a review of the objectives is possible. The objectives for this work included:

1. Verify the physics within the CFD software agrees with the expected results for the problem presented. The verification can be done by comparing the velocity and temperature profiles of the fluid within the simulation to the expected trends for both the temperature and velocity profiles.
2. Create a procedure using the global rotation method that users can follow to determine the heat transfer coefficient due to the rotation of the disk. The results from the procedure must agree with published results. In addition, the procedure must use the information gathered from the verification process. Mainly, the procedure must outline the size of the computational domain.
3. Create a secondary procedure using the local rotation (sliding) method to ensure that the CFD software is displaying the correct results and that this secondary procedure also agrees with published results.
4. Compare the global rotation and local rotation (sliding) method for accuracy to provide insight as to which method is better for applications.
5. Expand the utilization of the best procedure to cover both low and high rotational speeds for a rotating disk while showcasing how the results compare with analytical solutions.

When verifying the CFD model, both the temperature and velocity profiles resembled the expected trends. The temperature profile ranges from maximum values near the surface of the disk to minimum values at distances far from the surface of the disk. The maximum temperature of the fluid was equal to the surface wall temperature of the disk, while the minimum temperature was equal to the initial ambient temperature of the fluid. The velocity profile followed a similar trend. The maximum value was at the surface of the disk, and the minimum value was found at locations far from the surface. The maximum value was equal to the tangential velocity, while the minimum velocity was equal to zero.

The global rotation method and the local rotation (sliding) method were successfully utilized to estimate the heat transfer coefficient of the fluid caused by the rotation of the disk. Both methods had percent differences below 3% for all mesh sizes that were tested. A procedure for each method was generated and showed the size of the computational domain. The size of the computational domain was found by considering the results of the verification process. Since both the velocity profile and temperature profile required the height of the domain to be above 1 meter, to accurately replicate the expected results, the computational domain had a height of 3 meters. The 3 meters is large enough to allow for testing in both the laminar and turbulent regime.

When comparing the global rotation method and the local rotation (sliding) method, the method that better represented the physical problem in question is the global rotation method. The global rotation method does not require the user to introduce a secondary body. The secondary body is the item rotating when using the local rotation (sliding) method. The secondary body causes inaccuracies to appear when discretizing the domain into cells. These inaccuracies cause the local rotation (sliding) method to be less predictable than the global rotation method. The unpredictability is seen when looking at the percent difference of the obtained heat transfer coefficient when the level of the initial mesh size was changed. When increasing the initial level of mesh size, the percent difference should decrease. However, this was not the case in all trials, and few trials had results where an increase in the mesh size increased the percent difference.

In contrast, when using the global rotation method, no unpredictable changes in percent difference were seen. The global rotation method approximates the effects of the rotating disk by considering the forces acting on the fluid as the fluid rotates and interacts with the disk. When obtaining results for the heat transfer coefficient of a singular body, the global rotation method is recommended. When obtaining results for combined sources of heat transfer, the local rotation (sliding) method is recommended.

For this work, a single rotating disk is being considered, so the global rotation method was used to obtain values for the turbulent and transition regime. For the turbulent regime, the values obtained were compared to reported results from the literature. The percent differences associated with the values found from the CFD simulation were below 3% for the turbulent regime. However, when

plotting the transition zone, the utilization of a constant for the turbulent parameters caused issues to arise. The precision of the results was not adequate at the low end of the transition zone. These issues can be avoided by using an equation to describe the turbulent parameters in terms of the fluid velocity.

Conclusions made from the results obtained for include the following

- An analysis of the velocity and temperature profiles within the CFD software allows for an approximate size of the computational domain to be determined before obtaining results for the convective heat transfer coefficient.
- Computational fluid dynamics software allows for accurate results when analyzing forced convective heat transfer caused by the rotation of a disk submerged in still air.
- The regimes that can be tested by using settings within the CFD software include the laminar and turbulent regimes.
- For both the laminar and turbulent regime, the simulation time is a function of the total number of cells raised to a power and multiplied by a constant.
- The percent difference in the laminar regime is an exponential function, while in the turbulent regime the percent difference is a natural log function.

Items to enhance the study include:

- Utilize an equation that relates the turbulent parameters to variables within the CFD domain.
- Generate an experiment with a disk containing holes and other imperfections and compare the experimental results to values obtained from CFD simulations.

## REFERENCES

- [1] Cobb, E., & Saunders, O. (1953). Heat transfer from a rotating disk. *Imperial College of Science and Technology*, 343-351.
- [2] Dorfman, L. (1968). *Hydrodynamic resistance and the heat loss of rotating solids*. Edinburgh: Oliver and Boyd.
- [3] Owen, J., Haynes, C., & Bayley, F. (1973). Heat transfer from an air-cooled rotating disk. *Mechanical Engineering Laboratories, School of Applied Sciences, University of Sussex*, 453-473.
- [4] Popiel, C., & Boguslawski, L. (1975). Local heat-transfer coefficients on the rotating disk in still air. *International Journal of Heat and Mass Transfer*, 167-170.
- [5] Malik, M., Wilkinson, S., & Orszag, S. (1981). Instability and transition in rotating disc. *AIAA*, 1131-1138.
- [6] Cardone, G., Astarita, T., & Carlomagno, G. (1997). Heat Transfer Measurements on a Rotating Disk. *International Journal of Rotating Machinery*, 1-9.
- [7] Latour, B., Bouvier, P., & Harmand, S. (2011). Convective Heat Transfer on a Rotating Disk With Transverse Air Crossflow. *Journal of Heat Transfer*, 133.
- [8] Trinkl, C., Bardas, U., Weyck, A., & aus der Wiesche, S. (2011). Experimental study of the convective heat transfer from a rotating disk subjected to force air streams. *International Journal of Thermal Sciences*, 73-80.
- [9] aus der Weishce, S., & Helcig, C. (2016). *Convective Heat Transfer From Rotating Disks Subjected To Streams Of Air*. New York: Springer.
- [10] Shevchuk, I. V. (2016). *Modelling of Convective Heat and Mass Transfer in Rotating Flows*. New York: Springer.
- [11] SolidWorks. (2018). *TECHNICAL REFERENCE SOLIDWORKS FLOW SIMULATION 2018*.